Energy 45 (2012) 1042–1058

Contents lists available at SciVerse ScienceDirect

Energy

journal homepage: www.elsevier.com/locate/energy

CO_2 capture using monoethanolamine (MEA) aqueous solution: Modeling and optimization of the solvent regeneration and CO_2 desorption process

Patricia Mores [a], Nicolás Scenna [a], Sergio Mussati [a,b,*]

[a] UTN – FRRo, Zeballos 1341, S2000BQA (Rosario), Argentina
[b] INGAR/CONICET, Instituto de Desarrollo y Diseño, Avellaneda 3657, 3000 Santa Fe, Argentina

ARTICLE INFO

Article history:
Received 9 November 2011
Received in revised form
1 May 2012
Accepted 14 June 2012
Available online 26 July 2012

Keywords:
CO_2 desorption
Simultaneous optimization
Mathematical programming
Amine regeneration

ABSTRACT

This paper deals with the simultaneously optimization of operating conditions (pressures, temperatures and flow-rates) and dimensions (diameter and height) of the amine regeneration unit in the post-combustion CO_2 capture process. The proposed model takes into account the effect of kinetic reactions on the mass transfer, the hydraulics of the random packing and the pressure drop along the column. In addition, profiles of temperature, composition and flow-rate along the height of the regenerator are also predicted.

The resulting mathematical model is implemented into the optimization environment General Algebraic Modeling System (GAMS) which is a high-level modeling system for mathematical programming and optimization. The benefits of the mathematical programming techniques (equation-oriented modeling tools) are exploited for the simultaneous optimization not only of the operating conditions but also the dimensions of the all piece of equipments (heat exchangers, regeneration unit, condenser and reboiler).

The mathematical model was successfully verified by comparison of the obtained results with published experimental data and simulated solutions obtained by a process simulator (HYSYS). Once validated, the model was used for optimization purpose.

Finally, in order to study the effect of the main process parameters on the optimized results a sensitivity analysis is also investigated and discussed in detail.

1. Introduction

The world's rapidly expanding population and growing industrialization in emerging economies lead to dramatically increase the energy consumption. Specialists predict that the world energy demand will increase at faster rate in the coming decades. Although there will be a shift towards alternative sources of energy, the dependence on fossil fuels will still remain dominant for the next decades.

Despite that renewable energy sources (nuclear, geothermal, solar, hydro and wind-driven generators) are *environmental* friendliness, they currently have very limited capacities, because the energy that they generate is still relatively expensive and at the same time, the generation process cannot be controlled. For example, the nuclear energy is a very clean source of energy, but the potential emergency hazard progressively reduces the number of newly-built nuclear plants.

From energy generation capacity point of view, it is clear that the exploitation of fossil fuels (mainly coal and natural gas) will still play an important role in the next decades. However, the *CO_2 levels emitted into* the atmosphere are too high and *affect the* environment *adversely*. In fact, the CO_2 emission is considered to be the main cause of the global warming and has been dramatically increased during the last years. Moreover, it is expected that *it will still grow by* almost 3% per year.

For this reason, many initiatives, actions and efforts are underway to reduce the greenhouses gas emissions coming from the burning of fossil fuels. Specifically in the electricity production sector, the attention is focused on the carbon capture and storage (CCS) technologies which are expected to play a key role to reduce carbon emissions.

At the moment, the following are three CO_2 capture processes which are being intensively studied: oxy-fuel combustion, pre-combustion and post-combustion. Each one of them has its own advantages, disadvantages and limitations. Full-scale CO_2 capture

* Corresponding author. INGAR/CONICET, Instituto de Desarrollo y Diseño, Avellaneda 3657, 3000 Santa Fe, Argentina. Tel.: +54 342 4534451; fax: +54 342 4553439.
E-mail address: mussati@santafe-conicet.gov.ar (S. Mussati).

0360-5442/$ – see front matter © 2012 Elsevier Ltd. All rights reserved.
http://dx.doi.org/10.1016/j.energy.2012.06.038

Nomenclature

a	Effective interfacial area for mass transfer, m^2/m^3
D	Diffusivity, m^2/s
DT	Tower diameter, m
E	Enhancement factor
ECO	Economizer
f	Flooding factor
G	Gas flow-rate, mol/s
G'	Gas mass velocity, kg/s m^2
H	Enthalpy, kJ/kmol
h	Stage height, m
H_{CO_2}	Solubility of CO_2 in MEA–H_2O solution
$H_{CO_2,i}$	Solubility of CO_2 in MEA or H_2O
ΔH_{H_2O}	Vaporization heat of water, kJ/kmol
ΔH_R	Reaction heat, kJ/kmol
HTU	Height of transfer units, m
K_m	Equilibrium constant of m reaction
k_r	Kinetic constant, mol/m^3
k^L	Liquid side mass transfer coefficient, m/s
k^G	Gas side mass transfer coefficient, kmol/Pa s m^2
L	Liquid flow-rate, mol/s
L'	Liquid mass velocity, kg/s m^2
LAC	Lean amine cooler
NTU	Number of transfer units
P	Pressure, kPa
p	Partial pressure, kPa
Q	Energy, kJ/s
T	Temperature, K
$u_{sg,z}$	Superficial velocity, m/s
u_{fz}	Flooding velocity, m/s
x	Mole fraction in liquid phase
y	Mole fraction in gas phase
ΔP	Pressure drop, kPa
η	Murphree efficiency
ρ	Molar gas density, $kmol/m^3$
ρ'	Mass density, kg/m^3
σ	Surface tension, N/m
σ_C	Packing surface tension, N/m
μ	Viscosity, kg/m s
γ	Activity coefficient
φ	Fugacity coefficient
α	CO_2 loading
λ	Stripping factor

Subscript

C	Condenser
R	Reboiler
LC	Lean cold amine
RC	Cold rich amine
RH	Hot rich amine
j	Gas component
i	Liquid component
H_2O	Water
CO_2	Carbon dioxide
MEA	Monoethanolamine
z	Stage "z"
m	Reaction

Superscripts

G	Gas phase
L	Liquid phase
*	Equilibrium condition

from power plants is not yet commercially mature, and research is needed in several research areas. The most promising technology is the post-combustion process where, after burning the fossil fuel in conventional combustors, the CO_2 is removed from a gas mixture, composed mainly by N_2 and H_2O, using amines. Certainly, it is expected that the CO_2 absorption/desorption process using chemical solvents will be the first capture process that will be ready for large-scale operation. It is, however, an energy intensive process because it requires high reboiler heat duty to regenerate the amine solution which is the main drawback of this technology. The reboiler energy requirement strongly depends on the CO_2 recovery, operating conditions of the regenerator (temperature, pressure) and the dimensions (diameter, height) as well as on the type of the column used: packed or tray column. Also, the characteristic of the amine solution (primary, secondary or tertiary amines) has a significant influence on the energy required for its regeneration. Therefore, the optimization of the stripping section in order to improve the energy efficiency is one of the major challenges of the post-combustion CO_2 capture. The optimization task should consider all trade-offs and interactions between the process variables.

Currently, there are several research issues which are being addressing to improve the performance of the regenerator unit. One of them is concerned with the selection and development of amine solvents with high absorption efficiency and low environmental impact and heat of absorption (and therefore the recovery heat requirements). Certainly, several *laboratory and bench scale tests* are being conducted to determine the effectiveness and competitiveness of several amines [1–12].

The study of the performance of CO_2 capture processes in pilot and demonstration scale plants is also an important research area. It is crucial to provide valuable insights into operating strategies (start-up, operational reliability, control and flexibility) of future full-scale plants, to obtain reliable data and to identify technical bottlenecks.

Another research area, which will be specifically addressed in this paper, is the modeling and optimization of CO_2 capture processes using advanced mathematical programming tools. They can be effectively used to gain insights and identify trade-offs between the process variables which help to determine feasible and optimal process designs. Certainly, process alternatives and modifications can be easily evaluated by reliable mathematical models in short times. Moreover, a list of experimental *tests* to be carried out in pilot or demonstration plants can be identified from simulation and/or optimization results obtained by solving mathematical models. Thus, mathematical models developed in a predictive way can be used as a complement to experimental research works.

Specifically in the area of amine based post-combustion, several simulation models with different levels of detail have been implemented in several process simulators (Aspen Plus, Aspen HYSYS, CHEMASIM, ProMax, ProTreat). Certainly a wide variety of models ranging from simplified equilibrium models to detailed rate based models have been developed in order to analyze the performance of the amine based capture [13–33]. By using these models and assuming the dimensions of columns as given and known, the authors carried out simulations in order to study the performance of the process including both thermodynamic and economic criteria. In addition, the implemented models were also used to optimize same operating variables via parametric simulation, that is, the models are solved several

times using different values of one or more operating variables (solvent recirculation, absorber and stripper temperature and pressure, among others) and the optimal values are obtained by inspection.

While process simulators allows users to easily predict the process performance in a short time without the need to define complex mathematical equations modeling the system, their use for simultaneous optimization is not a straightforward task as it demands for considerable manual and trial-and-error efforts by the user to adjust the variables to attain the objective function and thus the trade-offs that there exist between the all the process variables are not considered simultaneously. In addition, because of the architecture of the process simulators, the rationality, accuracy and precision of the results are strongly influenced by the number of variables and recycles presented in the process; the higher number of variables the lower accuracy and precision of the results. In contrast to this, the application of mathematical programming models for the optimal synthesis (process configuration) and design is more convenient than the use of process simulators. Certainly, significant advances have taken place with this methodology, which offers the possibility of developing automated tools to support the exploration of alternatives and optimization of chemical processes by design engineers. Thus, mathematical programming tools such as General Algebraic Modeling System (GAMS), A Mathematical Programming Language (AMPL), general PROcess Modeling System (gPROMS), among others, have shown to be powerful and the optimality capacities of such tools are greater than simulator's capacities, especially when the optimization problem is large, combinatorial and highly non-linear.

This paper deals with the modeling and simultaneous optimization of the amine regeneration process which is considered to be the most energy-demanding part of the post-combustion process using amines. In contrast to a great number of articles addressing the simulation and optimization of CO_2 capture process using process simulators, this paper exploits the benefits of the use of the mathematical programming techniques to develop an equation-oriented mathematical model in order to simultaneously optimize not only of the operating conditions but also the dimensions of all piece of equipments. To the authors' knowledge, this issue has not been previously reported in the literature.

Precisely, a phenomenological and predictive *steady state* model is developed Certainly the proposed rate based model of the regenerator unit is developed via mathematical programming and is based on mass, energy and momentum balances taking into account the reaction kinetics and mass transport of each one the reacting species. Detailed correlations are also used to compute the pressure drop and dimensions of the column (diameter and height).

The resulting mathematical model can be used not only for optimization purposes but also for simulation purposes when the number of degrees of freedom for the system of equations is zero. In fact, the proposed model was first used as simulator for validation purpose. The output results were successfully compared with the available experimental data and results obtained from HYSYS simulator. Once the model was successfully validated, it was used as optimizer in order to maximize an objective function defines as the ratio between the amount of CO_2 captured and the reboiler heat duty. In addition, the effect of the main process parameters on the process efficiency is also investigated.

The mathematical model to be presented in this paper *is the first basic step of a more* ambitious project aimed at determining the optimal synthesis and design of electricity power plant including the capture of the CO_2 due to the fuel combustion. The final goal is to develop a mathematical model which will be combinatorial in nature and which will be based in a superstructure where all the alternatives of interest will be embedded and optimized simultaneously. Thus, the model should be robust and flexible enough for optimization purpose. Until now, the resolution of such complex problem using advanced mathematical programming tools (GAMS, AMPL gPROMS) has not been addressed in the scientific community.

The paper is outlined as follows. Section 2 briefly describes the CO_2 desorption process. Section 3 introduces the problem formulation. Section 4 summarizes the assumptions and the mathematical model. Section 5 presents applications of the developed NLP model and results analysis. Finally, Section 6 summarizes the conclusions of the paper.

2. Process description

A schematic flow-sheet of the regeneration process to be addressed in this paper is shown in Fig. 1. It basically consists of the following equipment.

1. Amine reboiler [REB]
2. Rich/Lean amine economizer [ECO]
3. Condenser and accumulator [COND]
4. Regeneration tower [REG]
5. Lean amine cooler [LAC]

As shown, the rich amine stream [RAS] coming from the absorption unit is preheated in a lean/rich cross heat exchanger [ECO] and then is pumped to the regenerator unit [REG] for the regeneration of the absorbent amine solution. For this, the CO_2-rich amine is heated in a reboiler [REB] using low-pressure steam in order to maintain the regeneration condition which leads to a high thermal energy penalty. In fact, the total heating energy supplied in the reboiler [Q_R] is used for: 1) sensible heat to increase the rich solution temperature leaving the absorber, 2) desorption heat required for removing the CO_2 absorbed in the amine solution and 3) vaporization heat for steam which acts as stripping gas. Then, the steam is recovered in the condenser [COND] and fed back to the stripper while the CO_2 stream leaving the condenser, which is a relatively pure product (approx. 99%), is then dried and compressed. On the other hand, the lean amine solution leaving the regenerator is cooled and sent back to the absorber.

The regeneration performance is strongly influenced by the conditions of the aqueous amine solution (temperature, composition and flow-rate), pressure and temperature in the reboiler, condenser and regenerator units. The CO_2 recovery target and the regenerator dimension strongly influence the efficiency of the regeneration process. Then, it is interesting to identify and quantify trade-offs that may exist between the process variables.

3. Problem statement

The proposed optimization problem can be stated as follows. Given the flow-sheet shown in Fig. 1 and rich solvent conditions (composition, temperature and flow-rate), the goal is to determine the optimal operating conditions and dimensions of the regenerator unit in order to maximize the regeneration efficiency. More precisely, the following two objective functions are proposed: a) energy requirement in the reboiler (minimization) and b) ratio between energy requirement in the reboiler and the CO_2 removed from the aqueous amine solution (minimization).

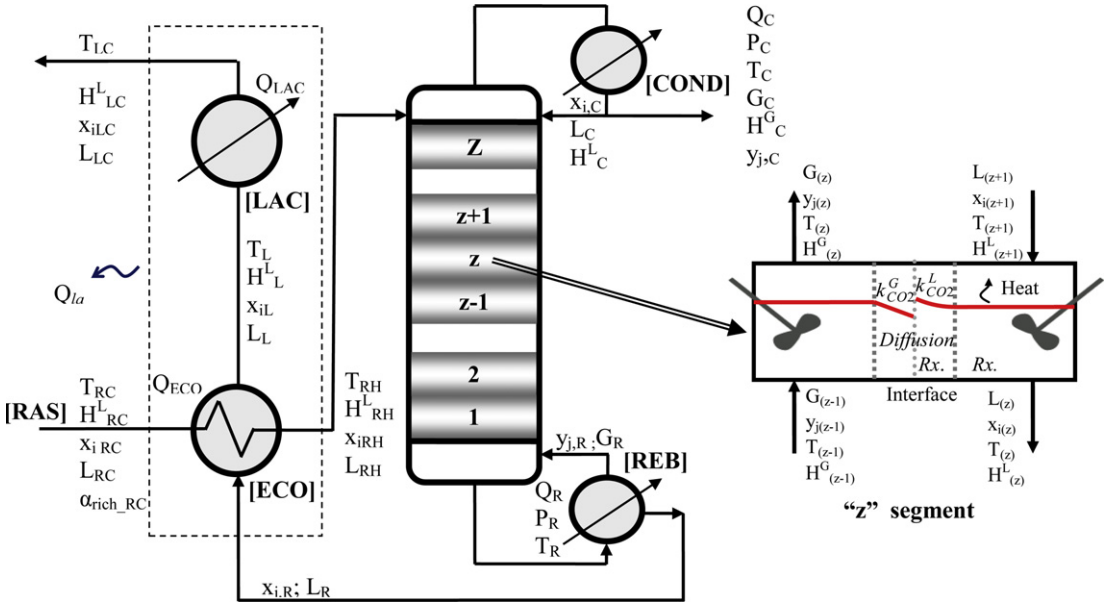

Fig. 1. Schematic flow-sheet of the CO_2 desorption process.

Formally, the optimization problem can be expressed as follows.

$$\text{To minimize subject to}: \begin{array}{l} F(x) \\ -)\ h_s(x) = 0\ \forall s \\ -)\ g_t(x) \le 0\ \forall t \\ -)\ \text{Design specifications} \end{array}$$

where x is the vector of the model variables. $F(x)$ and $h_s(x)$ refer, respectively, to the objective function and equality constraints (mass and energy balances, correlations used to compute physical/chemical properties, pressure drops, among others); $g_t(x)$ refers to inequality constraints which are used, for example, to avoid temperature crosses and to impose lower and upper bounds in some of the operating variables.

As will be described later, three different optimization problems are proposed and the obtained results are discussed in three case studies. The optimization problems differ depending on the objective function used and also on the varied model parameters in each case study.

The following are the main model variables which are optimized simultaneously and are obtained as output results: a) CO_2 recovery target, b) packing volume which depends on the height and diameter of the stripper, c) reboiler temperature, d) condenser pressure and temperature, e) heat loads in reboiler, condenser, lean-rich economizer and lean amine cooler, f) profiles of temperature, composition and flow-rate in liquid and vapor phases along the height of the regenerator. On the other hand, the main model parameters are: a) aqueous amine solution conditions (flow-rate, composition and temperature), CO_2 loading factor. In some optimization problems the reboiler pressure and the CO_2 recovery are considered as parameters (fixed and known values) but in others they are considered as decision variables.

Exploiting the robustness and flexibility of the proposed model, the influence of the main process parameters on the regeneration performance is also investigated for each one of the optimization problems.

4. Assumptions and mathematical model

The rate based model of the amine regeneration unit in the CO_2 absorption/desorption process developed in this work is described in detail in Appendix 1. Fig. 1 includes the nomenclature used to derive the mathematical model.

The main modeling assumptions are briefly exposed in this section.

As shown in Fig. 1, the height of the regeneration unit is divided into a given number of segments (Z) assuming that liquid and gas phases in each one of the segments are well mixed. Basically, each stage can be described by a set of equality and inequality constraints, which include mass and energy balances and specific correlations to compute thermodynamic properties, liquid and gas side mass transfer coefficients, effective area for mass transfer, column pressure drop, column diameter and height, stage effectiveness (Murphree's equation), kinetically controlled reaction rates, Vapor–Liquid Equilibrium (VLE) and chemical equilibrium relationships, fugacity coefficients, among others.

The model also considers the mass and energy balances corresponding to the condenser, heaters and reboiler. Condenser and reboiler units are modeled as equilibrium stages.

The following chemical reactions are considered:

$$2H_2O \leftrightarrow H_3O^+ + OH^- \quad \text{(R1)}$$

$$2H_2O + CO_2 \leftrightarrow H_3O^+ + HCO_3^- \quad \text{(R2)}$$

$$H_2O + HCO_3^- \leftrightarrow H_3O^+ + CO_3^{2-} \quad \text{(R3)}$$

$$H_2O + MEAH^+ \leftrightarrow H_3O^+ + MEA \quad \text{(R4)}$$

$$MEAH + HCO_3^- \leftrightarrow H_2O + MEACOO^- \quad \text{(R5)}$$

$$MEA + CO_2 + H_2O \leftrightarrow MEACOO^- + H_3O^+ \quad \text{(R6)}$$

$$CO_2 + OH^- \leftrightarrow HCO_3^- \quad \text{(R7)}$$

Kinetically controlled reactions (R6) and (R7) are assumed to occur in the liquid film while the bulk fluid remains in chemical equilibrium (R1)–(R5). According to the literature, a pseudo first-order reaction is assumed for reactions (R6) and (R7). The influence of the chemical reaction on the mass transfer rate is considered by an enhancement factor.

In addition, the effects of ionic strength solution are considered into determining CO_2 solubility (Henry's constant) in MEA solution. On the other hand, ideal behavior in liquid phase is considered, and consequently, activity coefficients are set to one.

Correlations to determine pressure drop and diameter of the column are also considered which depend on the gas flooding velocity as well as fluid properties and packing characteristics. The pressure drops along the heat exchangers are neglected.

Lower and upper bounds to allowable pressure drop, stage efficiency and percentage of flooding are defined. The height of the column is determined by the transfer model method (height and number of transfer units).

The proposed mathematical model, associated with continuous variables and highly non-linear and non-convex restrictions (bilinear terms, logarithms etc.), is formulated as an NLP model. It should be noticed that global optimal solutions cannot be guaranteed due to the non linear nature of the model.

The optimization model involves approximately 1500 variables and constraints. The model is implemented in GAMS [34]. The generalized reduced gradient algorithm CONOPT 2.041 is here used as NLP solver [35].

5. Results and discussion

5.1. Model validation

Only for validation purpose, the model was used as a simulator in a predictive manner, that is, no parameters were fitted to the experimental data.

As mentioned, the **model validation was performed by** comparing the simulated results with experimental data taken from the literature [12]. In fact, twenty-four runs reported in [12] have been used. The input data used in each one of the runs are listed in Table 1.

In order to emulate the pilot plant used in [12], the flow-sheet showed in Fig. 1 was slightly modified. For example, the reflux stream coming from the condenser [COND] had to be heated before returning to the stripper.

Table 1
Experimental operating conditions reported in Ref. [12].

Run	Stripper feed (rich amine solution)			Regenerator unit
	Molar flow [L_{RC}, mol/s]	CO_2 loading [$\alpha_{rich-RC}$]	Temperature [T_{RC}, K]	Condenser temperature [T_C, K]
1	14.08	0.42	368.11	284.05
2	14.03	0.405	368.16	284.00
3	9.66	0.457	368.96	283.15
4	9.73	0.433	366.96	283.15
5	21.62	0.525	364.05	284.96
6	21.69	0.523	365.56	285.00
7	27.41	0.496	346.68	286.85
8	27.48	0.493	347.27	287.56
9	21.05	0.532	353.91	293.57
10	21.02	0.533	354.37	291.33
11	18.02	0.537	358.00	294.85
12	17.79	0.491	359.61	288.00
13	41.76	0.496	345.63	286.37
14	41.77	0.506	345.22	286.45
15	59.48	0.546	344.95	287.02
16	59.67	0.507	346.11	287.71
17	59.21	0.508	345.13	287.67
18	21.03	0.493	362.83	285.76
19	21.19	0.413	362.37	285.30
20	17.75	0.386	370.08	284.26
21	16.54	0.54	370.06	284.20
22	14.75	0.495	368.99	283.47
23	14.74	0.538	369.26	283.61
24	27.40	0.506	351.00	284.98

Table 2
Packing specifications and regenerator's dimensions used for validation.

Column Type	Packed
Diameter (m)	0.427
Total packing height (m)	6.1
Stages number	10
Packing specifications	
Type of packed	IMTP#40
Specific area (m^2/m^3)	145
Nominal packing size (m)	0.04
Void fraction	0.97

Table 2 lists the packing specifications and regenerator's dimensions used for validation.

Figs. 2–6 show the comparison of the numerical values of the most important process variables corresponding to the experimental data listed in Table 1 (twenty-four runs) and the values predicted by the developed model. The comparison is made in terms of: a) total amount of CO_2 captured from the rich amine, b) reboiler heat duty, c) CO_2 loading in the lean amine solution (α_{lean}), d) CO_2 loading in the middle of the stripper (α_{middle}) and e) reboiler temperature. In addition, output results obtained by using two different correlations to compute the specific area for mass transfer [36,37] are also compared in order to study their effects on the performance of the model.

From the results shown in Fig. 2 it can be clearly seen that the experimental values of the CO_2 mass flow-rate for all runs are quite accurately predicted by the proposed model using both correlations and HYSYS simulator as well. For runs 1–11 the values of CO_2 mass flow-rate are overestimated when the Onda's correlation is used.

The following figures compare the predicted values and the experimental data for the CO_2 loading of each one of the runs at the bottom and middle of the regenerator unit. As is clearly shown in Fig. 3 the proposed model using the Bravo's correlation predict accurately the experimental data of CO_2 loading corresponding to all runs, excluding runs 19 and 20. Also, it can be observed that the accuracy of the values predicted by the Onda's correlation is different for each one of the experimental runs; for example, the

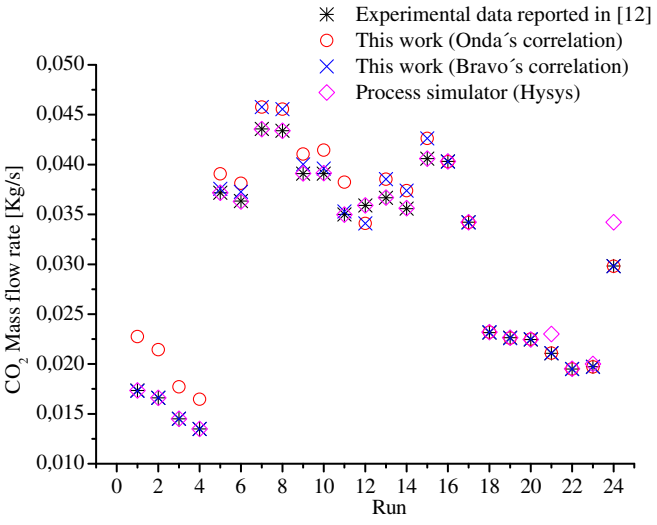

Fig. 2. Comparison between predicted and experimental values of CO_2 mass flow-rate (validation).

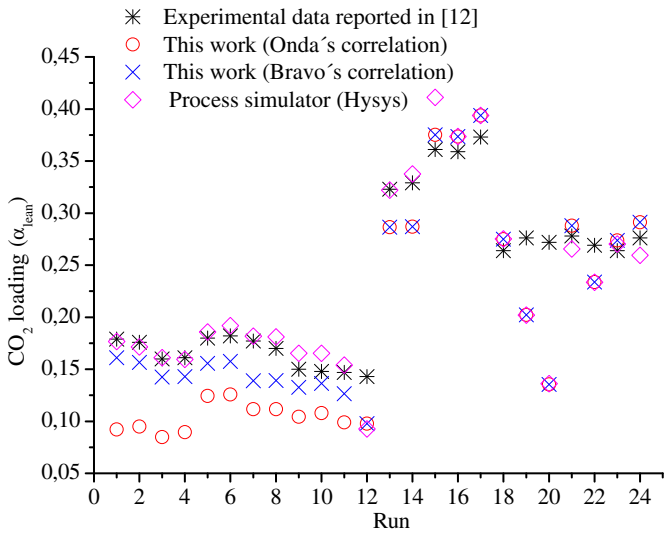

Fig. 3. Comparison between predicted and experimental values of CO_2 loading at the bottom of the regenerator (validation).

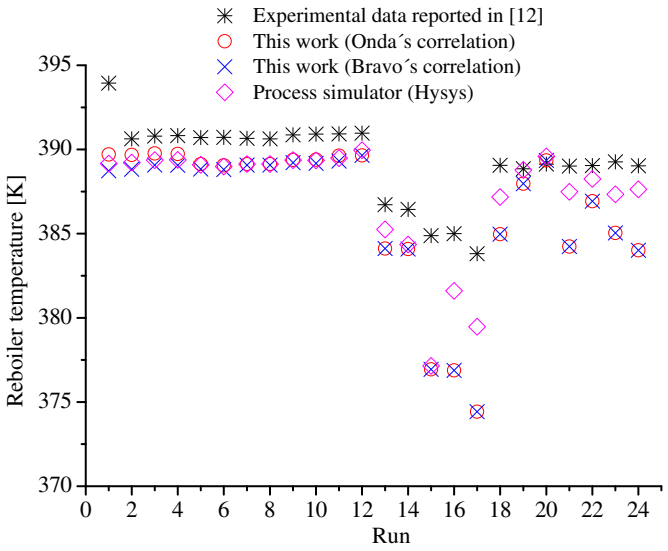

Fig. 5. Comparison between predicted and experimental values of reboiler temperature (validation).

experimental values of CO_2 loading for runs 14–24, excluding runs 19 and 20, are more accurately predicted than those corresponding to runs 1–13. The average relative difference between the predicted and experimental values for runs 1–13 and runs 14–24 are, respectively, 1.50–2.00% and 2.50–3.00%. For runs 1–11, the CO_2 loading values predicted by the Bravos's correlation are in better agreement with experimental data than those predicted by Onda's correlation, as in the case of the CO_2 mass flow-rate (Fig. 2). It is interesting to mention that for the experimental runs for which the CO_2 loading values are not well predicted (runs 12, 19 and 20), the numerical values predicted by the proposed model and HYSYS simulator are similar. Finally, it can be seen in Fig. 3 that, for all runs except for runs 12, 19 and 20, the experimental CO_2 loading values are correctly predicted by the HYSYS simulator.

Similar qualitative conclusions for CO_2 loading can be also observed at the middle of the regenerator for the majority of the runs (Fig. 4).

Figs. 5 and 6 compare the experimental and predicted values for the temperature and the heat duty in the reboiler. As shown in Fig. 5, 21 of 24 experimental temperature values are accurately predicted by the proposed model using both correlations. Certainly, the difference between the experimental and predicted values for runs 2–14, runs 19–20 and runs 22 is lower than 2 K while for runs 1, 18, 23 and 24 is around 6 K. On the other hand, only three experimental values (runs 15, 16 and 17) are not correctly predicted by both correlations; the difference between the experimental and predicted values is about 9 K.

On the other hand, experimental data of reboiler heat loads for some runs are better predicted than others. In fact, the experimental values for runs 12–24 are well predicted by the proposed model using both correlations. But the experimental values corresponding to runs 1–11, except runs 3 and 4, are not correctly predicted showing different behaviors depending on the correlation used. For example, as shown in Fig. 6, the experimental values

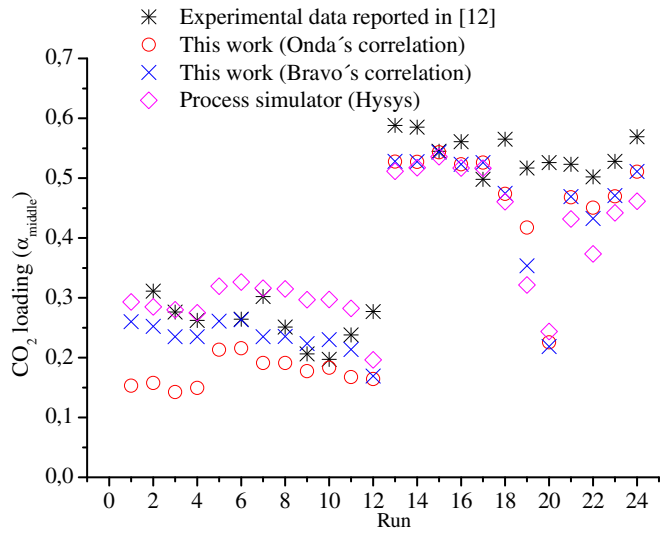

Fig. 4. Comparison between predicted and experimental values of CO_2 loading at the middle of the regenerator (validation).

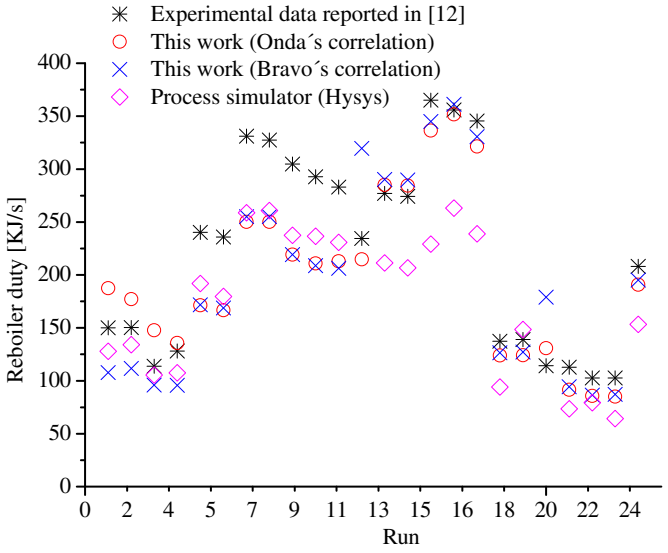

Fig. 6. Comparison between predicted and experimental values of reboiler heat duty (validation).

corresponding to runs 1–2 are overestimated and underestimated by the Onda's and Bravo's correlation respectively and the numerical differences between the experimental and predicted values are similar in both cases. On the other hand, the reboiler heat load of run 3 is more accurately predicted by the Bravo's correlation (slightly underestimated) while Onda's correlation predicted a better value for run 4 (slightly overestimated). Then, both correlations predicted similar values from runs 5 to 11 which are far from the experimental values. At this point it should be mentioned that the measurements of the heat duties of the reboiler corresponding to some runs may be subject to uncertainty due to the inherent limitations in the instruments used, as explained in detail in [12]. Table 3 lists the percentage errors (difference between the experimental and predicted values) of the most representative process variables: specific reboiler heat load, liquid flow-rate leaving the regenerator and reboiler and condenser temperatures. The reported data are useful to select the more suitable correlation to describe the steady state of the amine regeneration. As is shown, both correlations lead to similar and acceptable errors on the liquid flow rate to absorber [L_{LC}] and reboiler and condenser temperatures [T_R, T_C]. However, in contrast to this, the errors on the predictions of the specific reboiler duty obtained from both correlations are different.

Despite that 18 of 24 experimental data are slightly better predicted by the Bravo's correlation, the remaining six experimental data are not correctly predicted by this correlation; these six experimental values are much more adequately predicted by Onda's correlation (Table 3). The comparison clearly shows that, for runs 5–11; 13–19; 21–24, the numerical differences between the values predicted by both correlations are insignificant (0.40–3.40%). However, considerable differences can be observed for runs 1–4, 12 and 20. Certainly, the average value of the difference for runs 1–4 is 15.00% and for runs 12 and 20 is 40.00%.

Therefore, based on the error associated to each one of the correlations on the measurements of the process parameters at the inlet and outlet of the regenerator unit, it is possible to conclude that Onda's correlation seems to be more suitable to predict the experimental values reported in Ref. [12].

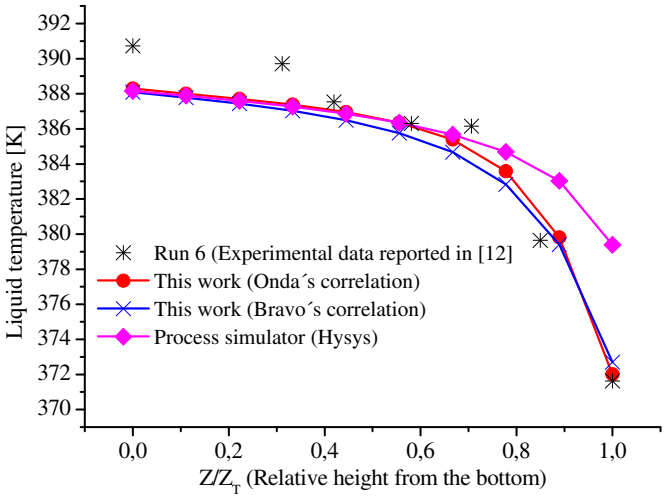

Fig. 7. Comparison between predicted and experimental profiles of liquid temperature for run 6 (validation).

For a more complete validation, the comparison of the profiles of liquid temperature inside the column predicted by the proposed model with experimental data was also investigated. Figs. 7 and 8 show the liquid temperature distribution along the height of the regenerator for runs 6 and 22. In both cases, seven experimental temperature values along the height of the regenerator are used for comparison.

As shown in Fig. 7, there is a good agreement between the simulated and experimental data for run 6. In fact, the results indicate that the output results obtained using Onda and Bravo's

Table 3
Deviations between predicted values and experimental data.

Run	Average deviation (%)											
	Specific reboiler duty [Q_R/kg CO_2 captured]			Liquid flow-rate to absorber [L_{LC}]			Reboiler temperature [T_R]			Condenser temperature [T_C]		
	This work (Onda's correlation)	This work (Bravo's correlation)	Hysys	This work (Onda's correlation)	This work (Bravo's correlation)	Hysys	This work (Onda's correlation)	This work (Bravo's correlation)	Hysys	This work (Onda's correlation)	This work (Bravo's correlation)	Hysys
1	4.7%	28.0%	14.7%	2.88%	2.18%	0.48%	1.08%	1.32%	1.21%	5.14%	3.94%	5.04%
2	8.8%	25.7%	10.8%	2.13%	1.50%	0.19%	0.24%	0.46%	0.36%	5.08%	4.23%	5.19%
3	6.3%	15.6%	7.1%	3.16%	2.55%	0.87%	0.26%	0.44%	0.36%	5.77%	5.09%	5.67%
4	13.1%	25.2%	16.0%	1.56%	1.00%	0.68%	0.28%	0.45%	0.37%	4.86%	4.36%	4.95%
5	32.1%	29.3%	20.1%	4.35%	2.96%	0.77%	0.40%	0.48%	0.41%	2.79%	3.01%	5.05%
6	32.7%	30.2%	23.8%	2.96%	1.21%	1.13%	0.43%	0.49%	0.44%	2.81%	3.00%	4.85%
7	28.1%	26.7%	21.8%	5.72%	3.89%	1.31%	0.39%	0.41%	0.39%	3.08%	3.20%	4.64%
8	27.2%	25.8%	20.3%	5.40%	3.55%	1.03%	0.38%	0.40%	0.39%	2.93%	3.06%	4.52%
9	31.5%	29.8%	22.2%	4.97%	3.66%	1.82%	0.38%	0.42%	0.38%	2.29%	2.44%	3.68%
10	32.1%	29.6%	19.2%	4.05%	3.04%	1.09%	0.39%	0.45%	0.40%	1.95%	2.14%	3.67%
11	31.2%	27.8%	18.4%	3.56%	3.25%	1.34%	0.33%	0.41%	0.37%	2.52%	2.71%	3.64%
12	3.5%	43.5%	19.5%	4.37%	4.37%	3.91%	0.34%	0.34%	0.26%	3.63%	4.74%	5.31%
13	2.1%	0.3%	23.7%	4.59%	4.59%	0.82%	0.67%	0.67%	0.38%	4.75%	4.75%	3.99%
14	1.3%	0.5%	24.7%	4.60%	4.60%	0.62%	0.61%	0.61%	0.54%	5.07%	5.07%	4.11%
15	12.2%	10.0%	37.3%	5.85%	5.85%	0.98%	2.06%	2.06%	2.01%	4.37%	4.37%	4.75%
16	1.1%	1.5%	26.1%	0.14%	0.14%	0.25%	2.11%	2.11%	0.88%	4.95%	4.95%	4.04%
17	6.9%	4.3%	30.9%	0.57%	0.57%	0.44%	2.44%	2.44%	1.13%	5.01%	5.01%	4.37%
18	10.0%	8.1%	31.7%	0.01%	0.01%	0.08%	1.05%	1.05%	0.49%	3.56%	3.57%	4.09%
19	10.4%	8.3%	6.8%	0.60%	0.60%	0.63%	0.23%	0.23%	0.02%	5.70%	6.74%	9.51%
20	14.2%	56.2%	37.3%	1.83%	1.83%	2.01%	0.05%	0.05%	0.12%	8.02%	9.31%	10.12%
21	18.9%	16.6%	40.3%	2.90%	2.90%	3.22%	1.23%	1.23%	0.39%	3.72%	3.74%	6.06%
22	16.4%	15.6%	22.7%	2.01%	2.01%	1.86%	0.55%	0.55%	0.21%	5.09%	5.85%	7.88%
23	16.8%	15.0%	38.2%	0.77%	0.77%	0.63%	1.08%	1.08%	0.49%	4.19%	4.25%	6.39%
24	8.3%	6.2%	35.8%	0.33%	0.33%	0.87%	1.29%	1.29%	0.36%	4.58%	4.58%	4.46%

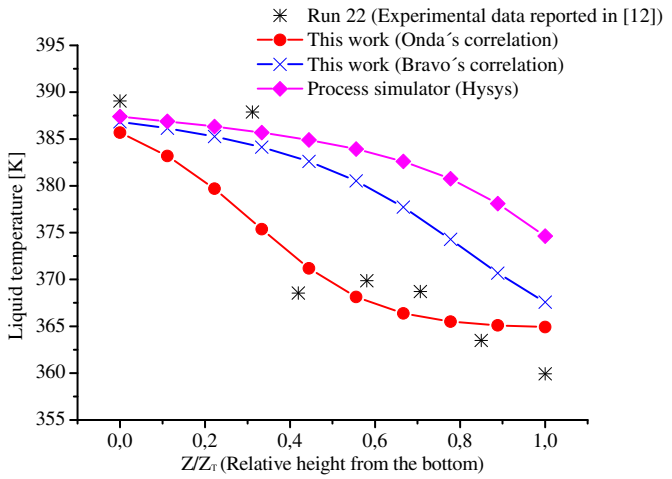

Fig. 8. Comparison between predicted and experimental profiles of liquid temperature for run 22 (validation).

correlations are quite similar. Similar conclusions have been obtained for runs 1–13. In contrast to the previous finding, Fig. 8 shows that for run 22 the values predicted by both correlations are only similar at the inlet and outlet of the regenerator but quite different inside the column. As shown, the experimental values from $z/Z_T = 0$ to $z/Z_T = 0.3$ are accurately predicted by the Bravo's correlation than Onda's correlation but from $z/Z_T = 0.4$ to $z/Z_T = 1$ the experimental values are better predicted by Onda's correlation than Bravo's correlation. Similar behaviors observed in Fig. 8 have been also observed for runs 17–24.

According to the simulated results, an interesting finding is the possibility of combining two correlations in order to compute the specific area for mass transfer in different sections of the regenerator unit for more accuracy and precision predictions of the profiles of temperature and compositions for all experimental runs: Bravo's correlation at the bottom of the regenerator and Onda's correlation from the middle to the top of the unit. This aspect is essential to study the unsteady-state and control strategies of the regeneration unit.

Then, based on the results listed in Table 3 and illustrated in Figs. 7 and 8, Onda's correlation will be used to compute the specific area for mass transfer for the optimizations that will be presented in the next sections.

5.2. Optimized results

The proposed mathematical model was used to solve the optimization problem stated in Section 3.

Precisely, the following three optimization problems listed in Table 4 have been solved.

As illustrated, the objective functions and the parameters assumed with their numerical values are the main difference between the optimization problems. The values assumed for each one of the parameters in each optimization problems are listed in Table 5. For instance, OP1 consists of minimizing the reboiler heat load [Q_R] by fixing L_{RC} (inlet liquid flow-rate), x_{i_RC} (inlet composition), T_{RC} (amine inlet temperature), P_R (reboiler pressure), three CO_2 recovery targets and α_{rich}. In contrast to OP1, OP2 and OP3 consider the CO_2 recovery as an optimization variable (continuous decision) and the objective function proposed in both cases is the specific heat load in the reboiler (minimization). In addition, in OP2 T_{RH} is considered as variable but is considered as parameter in OP3. In all optimization problems, α_{rich_RC} is varied from 0.30 to 0.55. Packing specifications of the regenerator unit are shown in Table 6.

As mentioned, the model is solved by varying several parameters. Then, the optimal values of the main process variables (energy requirements, regenerator dimensions, pressure drop, flow-rates and temperatures in condenser and reboiler as well as CO_2 stripper recovery, among others) for each one of the case studies are shown in terms of the assumed parameters in separate figures.

5.2.1. Optimized results obtained for case study 1. Influence of the CO_2 captured and α_{rich} on the energy requirements, total packing volume, condenser and reboiler temperatures and flow-rates

The optimal values obtained for each value of α_{rich_RC} and CO_2 recovery corresponding to the study case 1 are shown from Figs. 9–15. It is important to keep in mind that the results are obtained by varying α_{rich_RC} (CO_2 mole fraction/MEA mole fraction) and keeping constant the MEA mole fraction; therefore the CO_2 concentration increases and H_2O decreases as α_{rich_RC} increases. As shown in Fig. 9, the specific heat duties [MJ/kg of CO_2 captured] in the reboiler and condenser for all CO_2 recovery targets decrease as α_{rich_RC} increases. From $\alpha_{rich\_RC} = 0.30$ to 0.39–0.40, both energy requirements decrease more rapidly than from $\alpha_{rich\_RC} = 0.39$–0.40 to 0.55. It can be also seen that a same specific heat load in the reboiler are obtained at $\alpha_{rich\_RC} = 0.39$–0.40 for the three CO_2 recovery targets. In contrast to the trends observed from

Table 4
Different optimization problems: OP1, OP2 and OP3.

OP1 (Case study 1)	OP2 (Case study 2)	OP3 (Case study 3)
Min. $f(x) = Q_{reb}$ subject to:	Min. $f(x) = Q_{reb}$/kg of captured CO_2 subject to:	Min. $f(x) = Q_{reb}$/kg of captured CO_2 subject to:
1) $h_j(x) = 0\ \forall j$ (j = Eqs. (A.1)–(A.38)	1) $h_j(x) = 0\ \forall j$ (j = Eqs. (A.1)–(A.38)	1) $h_j(x) = 0\ \forall j$ (j = Eqs. (A.1)–(A.38)
2) $g_i(x) \le 0\ \forall i$ (i = Eqs. (A.39)–(A.42)	2) $g_i(x) \le 0\ \forall i$ (i = Eqs. (A.39)–(A.42)	2) $g_i(x) \le 0\ \forall i$ (i = Eqs. (A.39)–(A.41)
3) Design specifications (L_{RC}, x_{MEA_RC}, α_{rich_RC}, T_{LC}, P_R, CO_2 capture level)	3) Design specifications (L_{RC}, x_{MEA_RC}, α_{rich_RC}, T_{LC}, P_R)	3) Design specifications (L_{RC}, x_{MEA_RC}, α_{rich_RC}, T_{LC}, P_R, T_{RH})

Table 5
Parameter values used in each one of the optimization problems.

Operating conditions	Case study 1	Case study 2	Case study 3
Inlet amine flow rate [L_{RC}, mol/s]	10,000	10,000	10,000
Inlet amine composition [x_{MEA_RC}, mole fraction]	0.1127	0.1127	0.1127
Rich loading [α_{rich_RC}, mole CO_2/ mole MEA]	0.30–0.55	0.30–0.55	0.30–0.55
Temperature of the solution to absorber [T_{LC}, K]	313.15	313.15	313.15
Water molar fraction [y_{H_2O-C}]	$y_{H_2O-C} \le 0.1$	$y_{H_2O-C} \le 0.1$	$y_{H_2O-C} \le 0.1$
Rich amine temperature [T_{RH}, K]	Variable $T_{RH} \le T_R - 10$	Variable $T_{RH} \le T_R - 10$	353.15; 363.15; 373.15
Reboiler pressure [P_R, kPa]	130.00	130.00; 150.95; 202.60	130.00
CO_2 captured [%]	40; 45; 50	Variable	Variable

Table 6
Packing specifications used for optimization.

Packing specifications	
Type of packed	Ceramic Intalox Saddles
Specific area (m^2/m^3)	118
Nominal packing size (m)	0.05
Packing factor (m^2/m^3)	121.4
Void fraction	0.78

$\alpha_{rich\_RC} = 0.30$ to 0.39–0.40, the results obtained for values of α_{rich_RC} higher than 0.39–0.40 indicate the specific heat load for CO_2 recovery = 50% are smaller than those required by CO_2 recovery = 45 and 40%. The main reason of this behavior is because of that the energy required for the CO_2 recovery desired becomes more significant than that required for the H_2O evaporation. Fig. 10 clearly shows how the amount of captured CO_2 and the heat supplied in the reboiler vary with α_{rich_RC}. It is possible to observe in this figure that the amount of captured CO_2 increases faster than the reboiler heat load with the increasing of α_{rich_RC}. Moreover, it is interesting to mention that there exists an optimal value of α_{rich_RC} for which the reboiler heat load is minimum. The optimal values of

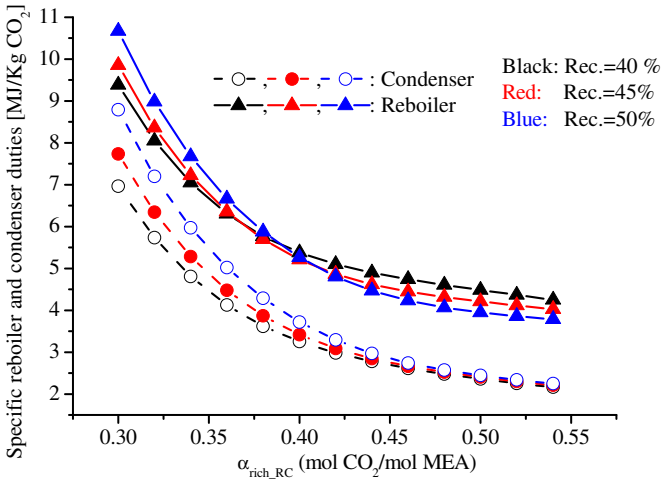

Fig. 9. Optimal values of specific heat loads in reboiler and condenser vs. α_{rich_RC} (case study 1).

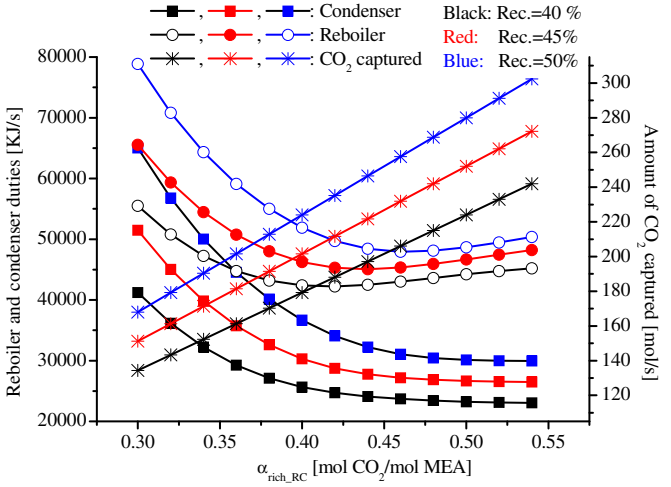

Fig. 10. Optimal values of reboiler and condenser heat loads and amount of captured CO_2 vs. α_{rich_RC} (case study 1).

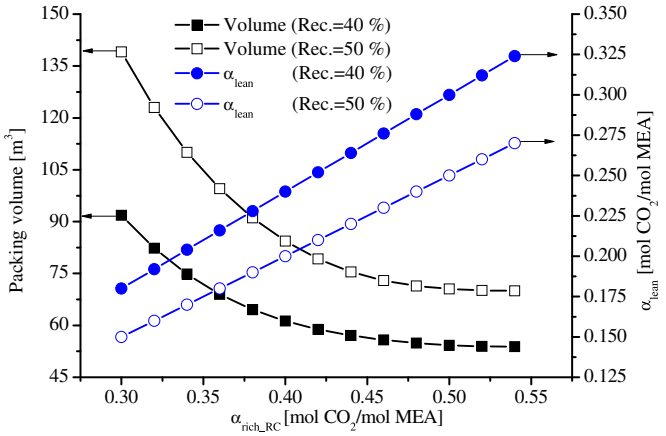

Fig. 11. Optimal packing volume and α_{lean} vs. α_{rich_RC} (case study 1).

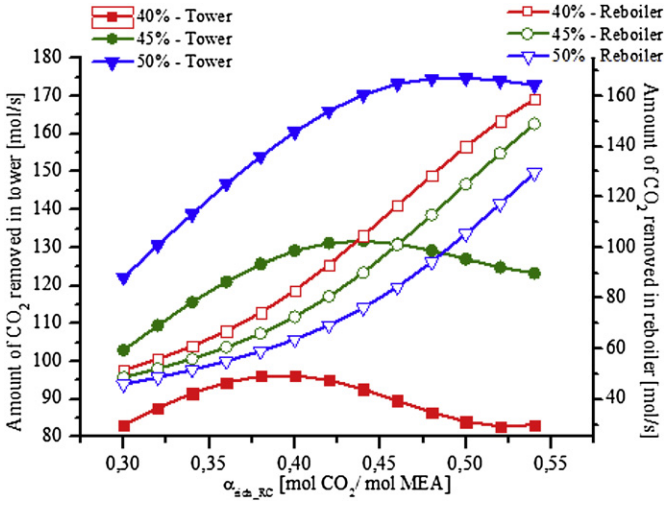

Fig. 12. Amount of removed CO_2 in reboiler and tower vs. α_{rich_RC} (case study 1).

α_{rich_RC} depend on the CO_2 recovery levels. For example, for CO_2 recovery = 40 and 50% the minimum reboiler heat loads (42,500.00 and 47,500.00 kJ/s) are obtained at $\alpha_{rich\_RC} = 0.40$ and 0.46 respectively.

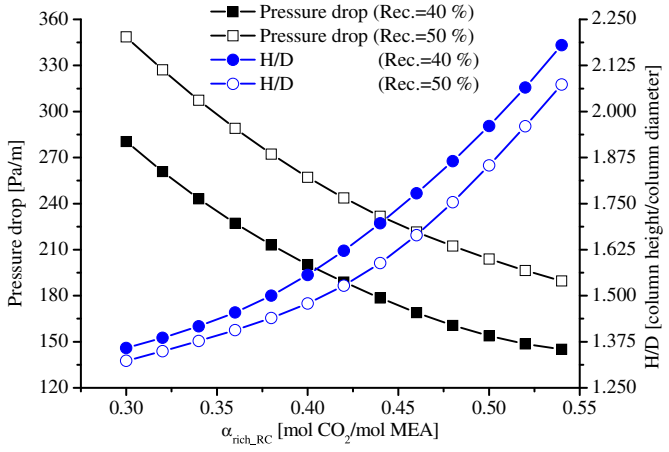

Fig. 13. Optimal pressure drop and H/D ratio vs. α_{rich_RC} (case study 1).

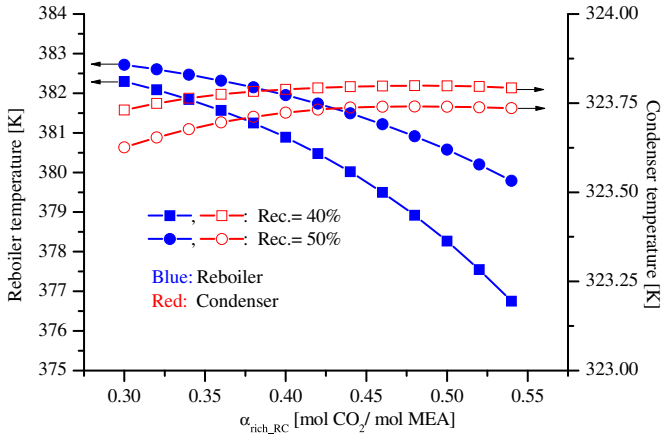

Fig. 14. Optimal reboiler and condenser temperatures vs. α_{rich_RC} (case study 1).

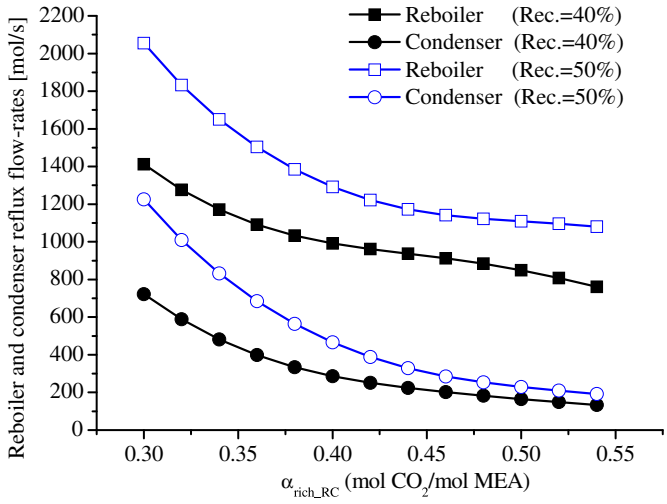

Fig. 15. Optimal reflux flow-rates in reboiler and condenser vs. α_{rich_RC} (case study 1).

In contrast to what is expected, Fig. 11 shows that the packing volume decreases as the amount of captured CO_2 increases. The packing volume decreases more rapidly from $\alpha_{rich\_RC} = 0.30$ to 0.39–0.40 than from 0.40 to 0.55. This can be explained based on

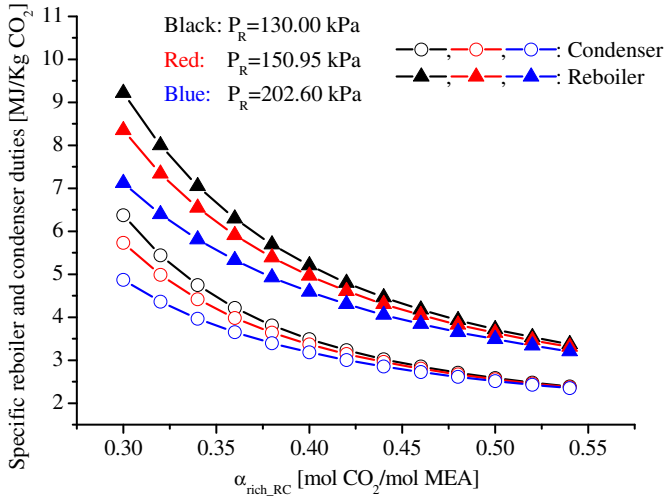

Fig. 16. Optimal values of specific heat loads in reboiler and condenser vs. α_{rich_RC} (case study 2).

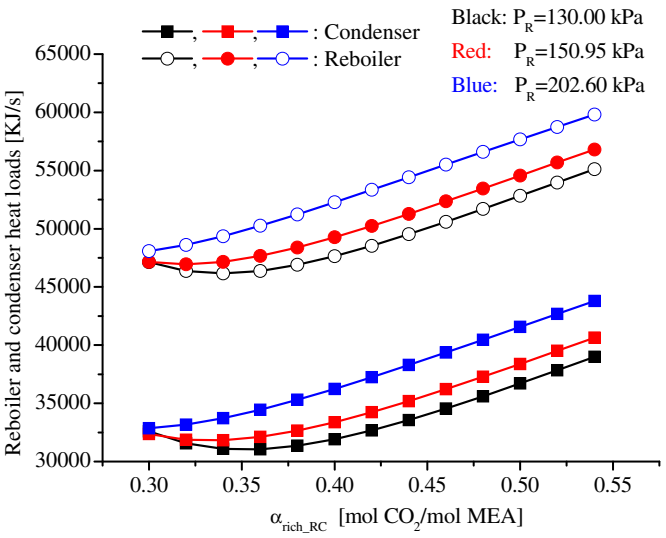

Fig. 17. Optimal values of reboiler and condenser heat loads vs. α_{rich_RC} (case study 2).

the fact that the CO_2 desorption is carried out in the regenerator unit and the reboiler as well. Fig. 12 shows the amount of CO_2 captured in the tower and in the reboiler for different CO_2 capture targets and α_{rich_RC}. It can be seen the importance of the reboiler in order to capture the desired amount of CO_2. In fact, for higher values of α_{rich_RC} than 0.42 the amount of CO_2 captured in reboiler increases significantly while the amount of CO_2 captured in the tower decrease slightly.

The corresponding optimal values of H/D ratios and total pressure drop for each value of α_{rich_RC} and CO_2 recovery are illustrated in Fig. 13. It can be clearly observed that the CO_2 recovery and α_{rich_RC} do not influence the trends of such variables. The total presssure drops decrease with the increasing of α_{rich_RC} while the H/D ratios increase as α_{rich_RC} increases. Finally, Figs. 14 and 15 illustrate the variation of the temperatures and reflux flow-rates in the reboiler and condenser [L_C and G_R]. As shown in these figures, for CO_2 recovery = 40.00 and 50.00%, the reboiler temperature decreases, respectively in about 2.00 K and 4.00 K as α_{rich_RC} increases from 0.30 to 0.55. The condenser temperature is not

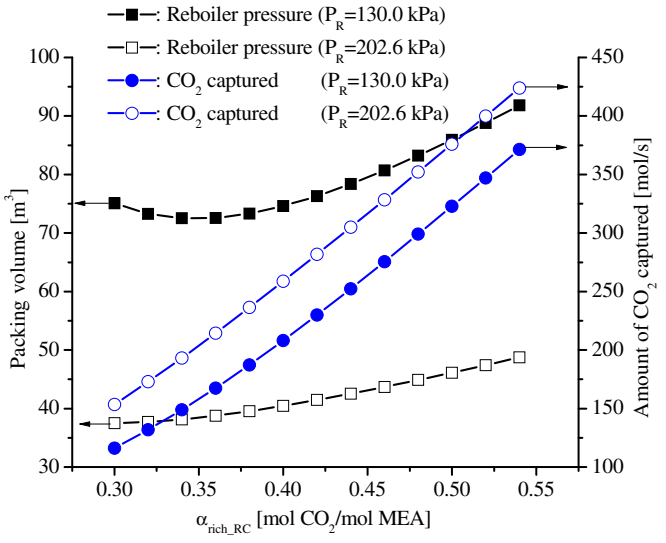

Fig. 18. Optimal packing volume and amount of captured CO_2 vs. α_{rich_RC} (case study 2).

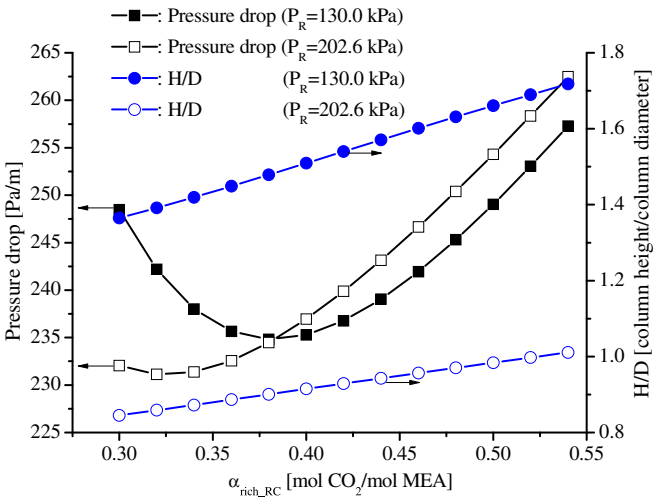

Fig. 19. Optimal pressure drop and H/D ratio vs. α_{rich_RC} (case study 2).

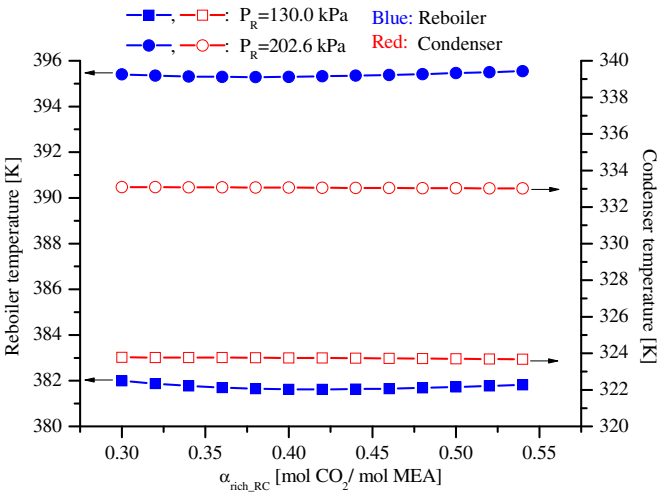

Fig. 21. Optimal reboiler and condenser temperatures vs. α_{rich_RC} (case study 2).

influenced by α_{rich_RC} and by the amount of CO_2 desired to be captured. The reason of this is that the condenser is assumed as an equilibrium stage and in all cases the water mole fraction ($y_{H_2O,C}$) reaches its upper bound (0.10). According to Fig. 15, the reflux flow-rates in the reboiler and condenser are more affected by the amount of CO_2 to be capured at low α_{rich_RC} values. Specifically, for $\alpha_{rich\_RC} = 0.30$ the smallest amount of CO_2 captured and the highest value of the specific reboiler heat duty are computed. Certainly, the greatest effect of the CO_2 recovery on both reflux flow-rates (reboiler and condenser) are observed at $\alpha_{rich\_RC} = 0.30$; the flow-rates in the reboiler and condenser required by CO_2 recovery = 50% are, respectively, 50 and 100% higher than those required for CO_2 recovery = 40%. Clearly, the higher the reflux flow-rates, the larger regenerator sizes (Figs. 11 and 15). Then, for values of α_{rich} higher than 0.35 the effect is reduced.

5.2.2. Optimized results obtained for case study 2. Influence of the stripper pressure and α_{rich_RC} on the energy requirements, total packing volume, condenser and reboiler temperatures and reflux flow-rates

The optimal solutions corresponding to the minimization of the specific reboiler duty varying the stripper pressure and α_{rich_RC} are presented from Figs. 16–21. In contrast to the previous study case, the amount of CO_2 captured is considered here as an optimization variable.

As expected, Fig. 16 shows that the specific heat loads in the reboiler and condenser decrease with the increasing of α_{rich_RC}. For low values of α_{rich_RC}, the stripper pressure has a significant influence on the specific heat loads in both pieces of equipments. For example, increasing the stripper pressure from 130.00 kPa to 202.60 kPa at $\alpha_{rich\_RC} = 0.30$, the specific heat load in reboiler and condenser could be reduced by 2.00 MJ/kg CO_2. In addition, the results presented in Figs. 18 and 19 clearly show the effect of the stripper pressure on the amount of the CO_2 captured and dimensions. In fact, the amount of CO_2 captured increases and the size of the stripper unit decreases with the increasing of the stripper pressure. Certainly, if the stripper pressure is 202.60 kPa, the amounts of CO_2 captured and the packing volume are, respectively, 24% higher and 48% smaller than those obtained if the stripper pressure is 130.00 kPa (Fig. 18). The differences of the amounts of CO_2 captured and the packing volume for both reboiler pressures kept almost constant when α_{rich_RC} is varied. However, higher temperature in the reboiler and condenser and higher reflux flow-rate in the reboiler are required when the stripper unit is operated at high pressure (Figs. 20 and 21).

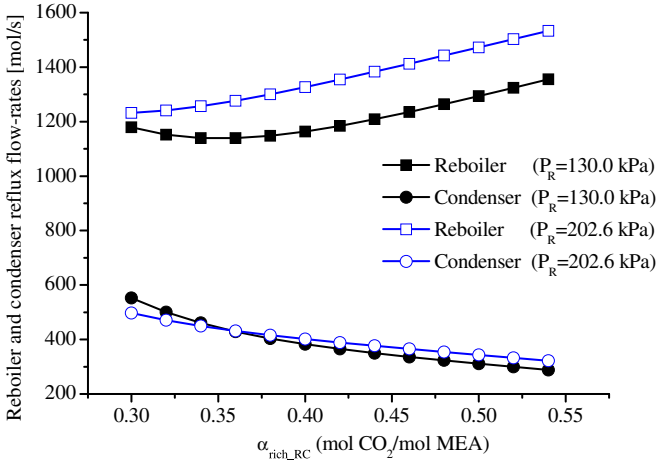

Fig. 20. Optimal reflux flow-rates in reboiler and condenser vs. α_{rich_RC} (case study 2).

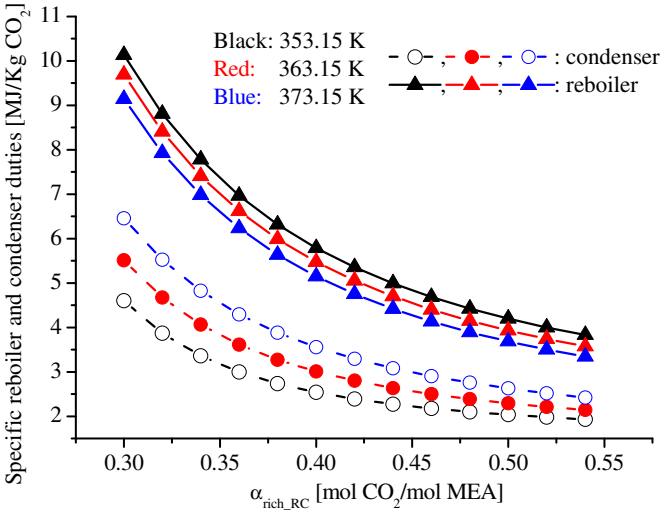

Fig. 22. Optimal values of specific heat loads in reboiler and condenser vs. α_{rich_RC} (case study 3).

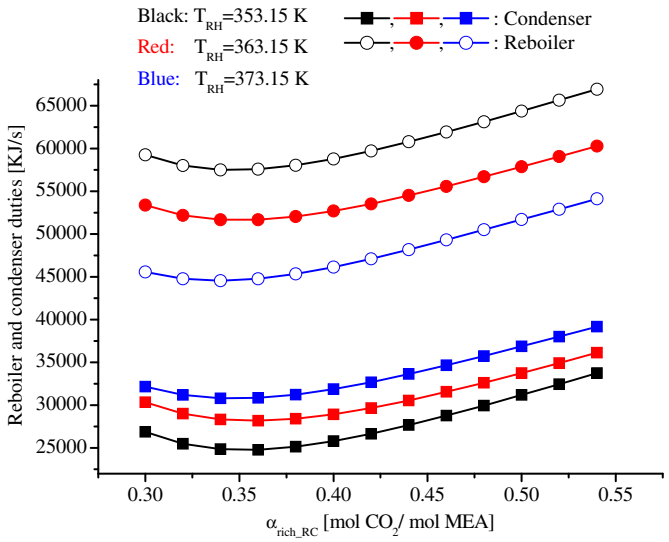

Fig. 23. Optimal values of reboiler and condenser heat loads vs. α_{rich_RC} (case study 3).

Figs. 20 and 21 show the influence of α_{rich_RC} and reboiler pressure on the reflux flow-rates in the reboiler and condenser as well as on their corresponding temperatures. As shown the reflux flow-rate in the condenser decreases as α_{rich_RC} increases and is not significantly affected by the reboiler pressure. In contrast to this, the reflux flow-rate in the reboiler increases with the increasing of α_{rich_RC} and is more affected by the pressure reboiler; higher reboiler pressures higher reflux flow-rates.

On the other hand, the temperature in reboiler and condenser increase 13 and 10 K respectively when the reboiler pressure is increased from 130.0 to 202.60 kPa (Fig. 21).

5.2.3. Optimized results obtained for case study 3. Influence of the rich amine temperature and α_{rich_RC} on the energy requirements, total packing volume, condenser and reboiler temperatures and reflux flow-rates

As in the previous study cases, Fig. 22 indicates that the specific heat loads in the reboiler and condenser decreases with the increasing of α_{rich_RC}. For a given value of α_{rich_RC} the minimum

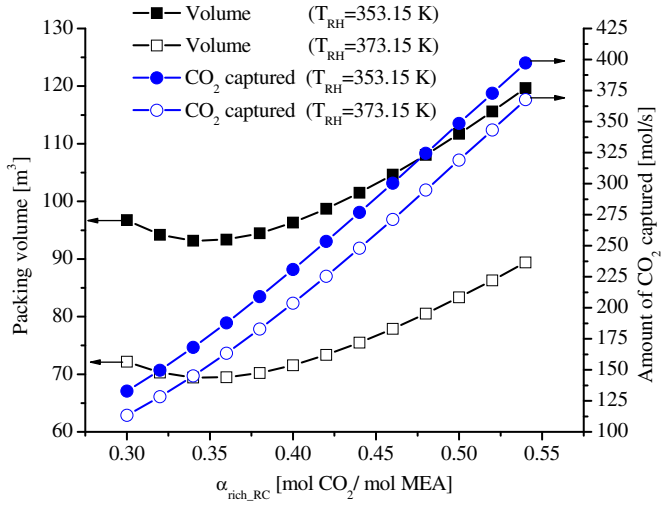

Fig. 24. Optimal packing volume and amount of captured CO_2 vs. α_{rich_RC} (case study 3).

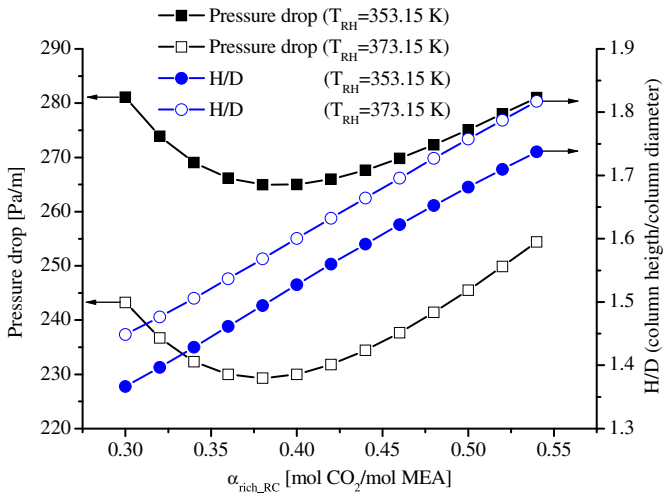

Fig. 25. Optimal pressure drop and H/D ratio vs. α_{rich_RC} (case study 3).

specific reboiler duty is obtained at higher rich amine temperature because the energy required to heat the amine solution up to T_R decreases as the rich amine temperature increases, independently of α_{rich_RC}. In addition, the amount of CO_2 captured at lower rich amine temperature is greater than that observed at higher rich amine temperature (Fig. 24). However, Fig. 23 clearly shows that the reboiler heat loads required are significantly greater. For example, for $\alpha_{rich\_RC} = 0.30$ and $T_{RH} = 373.15$ K, the heat load in the reboiler and the corresponding amount of CO_2 captured are, respectively, 46,000.00 (MJ/s) and 112.5 (mol/s) which lead to a minimum specific reboiler duty of 9.20 (MJ/kg CO_2 captured). On the other hand, for $\alpha_{rich\_RC} = 0.30$ and $T_{RH} = 353.15$ K, the heat load in the reboiler and the amount of CO_2 captured are, respectively, 68,000.00 (MJ) and 137.5 (mol/s) which lead to a minimum specific reboiler duty of 10.5 (MJ/kg CO_2 captured). According to this, the heat load in reboiler is increased in 47.00% and the amount of CO_2 captured is decreased in 9.00% when the rich amine temperature is varied from 373.15 to 353.15 K.

The specific heat load in the condenser is affected by the rich amine temperature in opposite way; the specific heat duty increases as the rich amine temperature increases. Certainly, for $\alpha_{rich\_RC} = 0.30$, it increases about 2 when the rich amine temperature increases from 353.15 to 373.15 K. It should be also mentioned that the difference on the specific heat loads in the

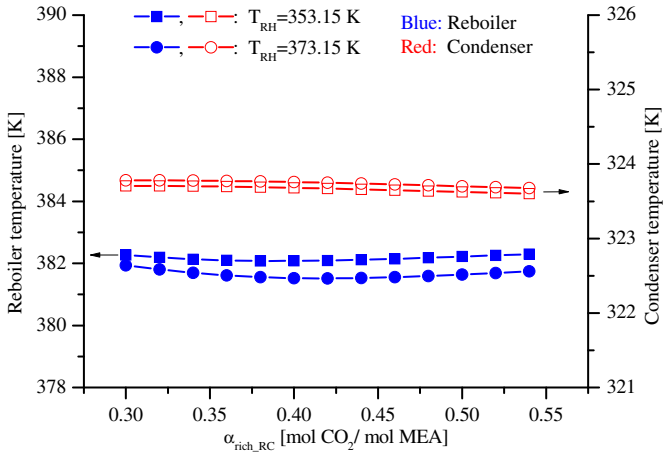

Fig. 26. Optimal reboiler and condenser temperatures vs. α_{rich_RC} (case study 3).

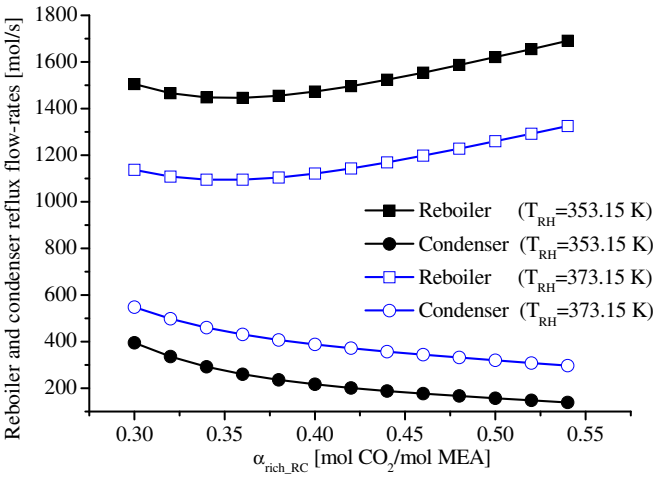

Fig. 27. Optimal reflux flow-rates in reboiler and condenser vs. α_{rich_RC} (case study 3).

condenser corresponding to 353.15 and 373.15 K decreases as α_{rich_RC} increases. For example, for $\alpha_{rich\_RC} = 0.30$ and 0.55 it decreases from 2.50 to 0.50. However, α_{rich_RC} does not affect the difference on the specific reboiler duty for two different rich amine temperatures.

Finally, Fig. 26 shows that T_{RH} does not affect the condenser and reboiler temperatures. The reflux flow-rate in the reboiler increases in about 33.33% when T_{RH} decreases from 373.15 to 353.15 K (Fig. 27). In contrast to this, the reflux flow-rate in the condenser decreases increases in about 47.15% when T_{RH} decreases from 373.15 to 353.15 K.

6. Conclusions and future works

A deterministic and phenomenological NLP mathematical model to study the CO_2 desorption from MEA aqueous solutions has been presented. Temperature, composition and flow-rate of liquid and gas streams along the height of the regenerator unit as well as dimensions including total pressure drop are considered as optimization variables. Depending on the *degrees of freedom of the equation system fixed by users*, the developed model is a valuable and useful tool not only *to optimize but also for simulate the desorption process*.

The output results have been successfully validated by comparing the predicted values with experimental data. From the verification results, the following key point to be addressed in future works, is closely connected with the development of more accurate models. It would be interesting to investigate the efficacy of developing a mathematical model using different correlations to compute the specific area for mass transfer in different section of the stripper; Bravo's correlation at the bottom of the regenerator and Onda's correlation from the middle to the top of the unit. The combination of both correlations may lead to predict better profiles of temperature and compositions for all experimental runs which are very important if the model is used to study the unsteady-state and control strategies of the regeneration unit.

After the model validation, three optimization problems considering different objective functions and design specifications have been solved. Certainly, for each one of the optimization problems, a set of optimal solutions for a wide range of the model parameters was presented and discussed. It should be here stressed that each one of the points plotted in Figs. 7–27 were simultaneously obtained.

In the case study 1 the operating conditions and dimensions have been obtained in order to minimize the energy requirement in the reboiler. In the other two study cases the ratio between the energy requirement in the reboiler and the amount of the CO_2 captured (specific heat load) has been minimized.

The effects of the main process parameters (reboiler pressure, α_{rich_RC}, rich amine temperature and CO_2 recovery levels) on the optimal solutions have been also investigated. Different concentrations of rich amine solution have been considered by varying the CO_2 loading factor (α_{rich_RC}). Trade-offs existing between the process variables for each one of the optimization problems have been also identified.

From the obtained results, the following are the main conclusions that can be observed for the three optimization problems (OP1, OP2 and OP3):

-) Values of α_{rich_RC} for which the total energy requirements (MJ/s) in the reboiler and condenser reach the minimum values. For instance, in OP1 the optimal values of α_{rich_RC} are 0.40 for CO_2 recovery = 40%, 0.42 for CO_2 recovery = 45% and 0.46 for CO_2 recovery = 50%.
-) As expected, the specific heat loads (MJ/kg of CO_2 captured) in the reboiler and condenser decrease as α_{rich_RC} increases.
-) Rich amine temperature, CO_2 recovery targets, reboiler pressure and α_{rich_RC} do not significantly affect the reboiler and condenser temperatures.

The following conclusions can also be drawn, depending on the optimization problem analyzed:

-) In OP1, the reflux flow-rates in the reboiler and condenser decrease with the increasing of α_{rich_RC}. In contrast to this, in OP2 and OP3 the reflux flow-rates in the reboiler increase as α_{rich_RC} increases.
-) In OP1, the reboiler temperature [T_R] decreases as α_{rich_RC} increases.
-) In OP2 and OP3, T_R kept almost constant when α_{rich_RC}, rich amine temperature and reboiler pressure are varied.
-) In OP2 and OP3, higher CO_2 recoveries, higher packing volumes.

An interesting conclusion can be observed from the optimized results which may be effectively applied for robust solution strategies. The optimal solution families presented for three optimization problems clearly show that the functionalities of the most important process variables (operating conditions and dimensions) with α_{rich_RC} are smooth (linear, polynomial, exponential decay, exponential growth) and therefore can be approximated correctly in a simple manner, without requiring detailed models. This finding is valuable because simple and empiric models (non-phenomenological models) involving the most important process variables can be derived to describe the tradeoffs existing between them. Then, the inclusion of such models in a systematic optimization procedure in order to solve complex and rigorous models is another advantage that can be exploited. In fact, it can be included in order to provide initial values and bounds for variables which may improve the convergence of large and phenomenological models.

Despite the good agreement between the model output results to those obtained by experimental works, the proposed model will be extended to improve the mass and energy transfer between phases and activity coefficients in order to remove the assumption about the ideality behavior in liquid phase. The rigorous optimization of the flow-sheet and design of electricity power plant including the capture of the CO_2 due to the fuel combustion will be also addressed. The resulting model will involve large number of discrete and continuous decisions.

Acknowledgments

Financial supports obtained from the Consejo Nacional de Investigaciones Científicas y Técnicas (CONICET), the Agencia Nacional para la Promoción de la Ciencia y la Tecnología (ANPCyT), the Universidad Tecnológica Nacional Facultad Regional Rosario (UTNFRRo) Argentina are gratefully acknowledged.

Appendix A

Mathematical model

The total height of regenerator is divided into Z stages. For model implementation, an index "z" is assigned for each one of the stages. Then, the mass, energy and momentum balances are derived using these indexes. Thus, by considering the assumptions presented in Section 4 and the defined notation, the following rate based model was derived for the complete regeneration amine aqueous process.

Regenerator unit [REG]

Mass and energy balances in stage "z"

$$L_{z+1}x_{i,z+1} - L_z x_{i,z} + G_R y_{j,R} - G_z y_{j,z} = 0 \quad z = 1 \tag{A.1}$$

$$G_{z-1}H^G_{z-1} - G_z H^G_z + L_{z+1}H^L_{z+1} - L_z H^L_z + (\Delta H_R)_z - (\Delta H_{H_2O})_z = 0 \; z = 1 \tag{A.2}$$

$$L_{z+1}x_{i,z+1} - L_z x_{i,z} + G_{z-1}y_{j,z-1} - G_z y_{j,z} = 0 \quad z = 2,..z.,Z-1 \tag{A.3}$$

$$L_{z+1}H^L_{z+1} - L_z H^L_z + G_{z-1}H^G_{z-1} - G_z H^G_z + (\Delta H_R)_z - (\Delta H_{H_2O})_z = 0 \quad z = 2,..z.,Z-1 \tag{A.4}$$

$$G_{z-1}y_{j,z-1} - G_z y_{j,z} + L_{RC}x_{i,RC} + L_C x_{i,C} - L_z x_{i,z} = 0 \quad z = Z \tag{A.5}$$

$$G_{z-1}H^G_{z-1} - G_z H^G_z + L_{RC}H^L_{RH} + L_C H^L_C - L_z H^L_z + (\Delta H_R)_z - (\Delta H_{H_2O})_z = 0 \; z = Z \tag{A.6}$$

where G and L are the gas and liquid flow-rate (mol/s), x and y are mole fraction of specie i (liquid phase) and j (gas phase), H^L and H^G are enthalpies for liquid and gas streams. ΔH_R and ΔH_{H_2O} are the heat released by the reaction and vaporization heat of water and the corresponding correlations are taken from Refs. [38,39], which are computed as follows:

$$-\Delta H_R = \text{mol of } CO_2 \text{ desorbed} \times R\left(1.428\times10^4 + 1.093\times10^6\frac{\alpha_z^2}{T_z} + 6.801\times10^6\frac{\alpha_z}{T_z} - 3.267\times10^4\alpha_z\right)$$

$$\Delta H_{H_2O} = \text{mol of } H_2O \text{ vaporized} \times 40.628\left[\frac{(Tc_{H_2O} - T_z)}{(Tc_{H_2O} - 373.15)}\right]^{0.38}$$

where Tc_{H_2O} is the water critical temperature [K] and α is the CO_2 loading, defined as the ratio between total CO_2 and total amine.

$$\left[MEAH^+\right]_z + \left[H_3O^+\right]_z = \left[MEACOO^-\right]_z + \left[HCO_3^-\right]_z + 2\left[CO_3^{2-}\right]_z + \left[OH^-\right]_z \tag{A.7}$$

where $[i]_z$ is the molar concentration of specie "i" in stage "z".

Chemical reactions and phase equilibrium relationship

The relationships of the equilibrium constants K_m of reactions (R1)–(R5) and Henry's coefficient ($H_{CO_2,i}$) with the temperature and composition are as below:

$$(K_m)_z = \prod_i (a_{iz})^{\nu_i} = \prod_i (x_{iz}\gamma_{iz})^{\nu_i} \quad \forall m,\ m = R_1,R_2,R_3,R_4,R_5 \tag{A.8}$$

$$(K_m)_z = \exp\left(A + \left(\frac{B}{T_z}\right) + C\ln(T_z)\right) \quad \forall m, m = R_1,R_2,R_3,R_4,R_5 \tag{A.9}$$

$$H_{CO_2,i,z} = \exp\left(A + \left(\frac{B}{T_z}\right) + C\ln(T_z) + DT_z\right) \forall i,\ i = \text{MEA},H_2O \tag{A.10}$$

T is absolute temperature (K) and a_{iz}, γ_{iz}, ν_i are activity, coefficient activity and stoichiometric coefficient to component "i" in reaction "m" respectively. The coefficients used in Eqs. (A.9) and (A.10) are taken from Refs. [40,41].

Phase equilibrium relationship

$$y_{CO_2,z}\varphi_{CO_2,z}P_z = H_{CO_2,z}[CO_2]_z \tag{A.11}$$

$$y_{H_2O,z}\varphi_{H_2O,z}P_z = p_{H_2O,z}x_{H_2O,z} \tag{A.12}$$

where φ_z, P_z and $p_{H_2O,z}$ refer to fugacity coefficient, total pressure and partial pressure of water, respectively. Fugacity coefficients are computed by using *Peng-Robinson equations* of state for multi-components [42]. Solubility of CO_2 in MEA solution (H_{CO2}), which is corrected for solution ionic strength, is taken from Ref. [43] and is computed as follows:

$$H_{CO_2\,z} = \left(10^{0.152I_z}\right)\left[\frac{x_{H_2O\,z}H_{CO_2MEA\,z} + x_{CO_2\,z}H_{CO_2\,H_2O\,z}}{\rho^L_z}\right] \tag{A.12a}$$

$$I_z = 1/2\sum_i \psi_i[i]_z \forall i,\quad i = MEAH^+, MEACOO^-, H_3O, OH^-, CO_3^{2-}, HCO_3^- \tag{A.12b}$$

where ψ_i is the ion charge.

Stage efficiency

Non-equilibrium stage is considered by incorporating an effectiveness term for the stage (η) through Murphree equation.

$$\eta_z = \frac{G_z y_{iz} - G_{z-1}y_{i\;z-1}}{G_z y^*_{iz} - G_{z-1}y_{i\;z-1}} \tag{A.13}$$

where $y^*_{i\,z}$ is the equilibrium composition of molecular specie considered leaving the stage z.

Stripper diameter

The diameter (DT_z) of each stage is computed as follows:

$$DT_z = \sqrt{\frac{4G_z}{u_{sg,z}\,\pi\rho^G_z}} \tag{A.14}$$

where ρ^G, G and $u_{sg,z}$ refer to the gas density, flow-rate and superficial velocity respectively. Then, $u_{sg,z}$ is related to the flooding velocity (u_{fz}) by Eq. (12):

$$u_{sg,z} = f_z u_{fz} \tag{A.15}$$

where f_z ranges from 0.65 to 0.70 (lower and upper bounds). Flooding velocity is estimated in terms of the packing factor, which depends on the type and size of packing, viscosities, densities and flow rates [44].

Stripper height

The height (h_z) of each stage is computed by the well-known unit transfer concept where:

$$h_z = \mathrm{HTU}_z \times \mathrm{NTU}_z \tag{A.16}$$

NTU_z and HTU_z refer to the transfer units and transfer unit height. Particularly,

$$\mathrm{HTU}_z = \left[\frac{G'_z}{R\,T_z\,a_z\,k_z^G\,\rho_z'^G}\right] + \lambda_z\left[\frac{L'_z}{k_z^L a_z \rho_z'^L E_z}\right] \tag{A.17}$$

where G', L' are gas and liquid mass velocities, ρ'^G and ρ'^L are gas and liquid mass densities, λ is the stripping factor ($\lambda = m/(L/G)$), k^G and k^L are the gas-side and liquid-side mass transfer coefficients, a is the effective interfacial area for mass transfer and E refers to the enhancement factor. A number of correlations exist for calculating the effective interfacial area for mass transfer. In this work, the proposed model was solved for two correlations in order to study the effect of such correlations on the validating case. Precisely, the following correlations proposed by authors in Refs. [36] and [37] are considered.

Correlation proposed by authors in Ref. [36]:

$$a_z = a_t\left(1 - \exp\left(-1.45\left(\frac{\sigma_c}{\sigma_z}\right)^{0.75}\left(\frac{L'_z}{a_t\mu_z^L}\right)^{0.1} \times \left(\frac{(L'_z)^2 a_t}{(\rho_z'^L)^2 g}\right)^{-0.05}\left(\frac{(L'_z)^2}{\rho_z'^L \sigma_z a_t}\right)^{0.2}\right)\right) \tag{A.18}$$

Correlation proposed by authors in Ref. [37]:

$$a_z = a_t 0.310\frac{\sigma_z^{0.5}}{h_z^{0.4}}\left(\left(\frac{\mu_z^L L'_z}{\rho_z'^L \sigma_z^L}\right)\left(\frac{6G'_z}{a_t\mu_z^G}\right)\right)^{0.392} \tag{A.19}$$

where A, σ, σ_c, u^G, M^L and h are cross-sectional area of column, liquid surface tension, surface tension of packing material, superficial gas velocity, liquid molecular weight and stage height, respectively.

The following constraint can be formulated by assuming that the liquid and vapor phases are well-mixed and point efficiency is equivalent to Murphree efficiency,

$$\eta_z = 1 - \exp(\mathrm{NTU}_z) \tag{A.20}$$

Total packing volume

$$\text{Packing Volume} = \sum_{z=1}^{Z}\pi\left(\frac{DT_z}{2}\right)^2 h_z \tag{A.21}$$

Amount of total CO_2 captured

$$\text{Amount of total captured } CO_2 = G_C y_{CO_2,C} \tag{A.22}$$

where $y_{CO_2,C}$ and G_C are the CO_2 mole fraction and gas flow rate (mol/s) of the condenser's gas stream.

CO_2 captured [%]

$$\text{Captured } CO_2[\%] = \frac{G_C y_{CO_2\_C}}{L_{RC} x_{MEA,R\ C}\alpha_{rich\_RC}} \tag{A.23}$$

where α_{rich_RC} is defined as:

$$\alpha_{rich\_RC} = \frac{x_{CO_2\_RC}}{x_{MEA\_RC}} \tag{A.24}$$

Enhancement factor

The influence of the reactions on the CO_2 transfer is considered by an enhancement factor (E) which is defined as follow:

$$E_z = \frac{\sqrt{\left(D_{CO_2}^L\right)_z\left[\left(k_{r,CO_2-MEA}\right)_z[MEA]_z + \left(k_{r,CO_2-OH}\right)_z[CO_2]_z\right]}}{k_z^L} \tag{A.25}$$

The forward constants (k_{r,CO_2-MEA} and k_{r,CO_2-OH}) of the parallel and kinetically controlled reactions (R6) and (R7) are taken from Refs. [40,45], respectively.

Pressure drop

The total pressure drop (ΔP) along the regeneration unit is given by:

$$\Delta P = \sum_z \Delta P_z h_z \tag{A.26}$$

Pressure drop in each stage (kPa/m) is estimated by the correlation proposed by authors in Ref. [46]. It takes into account the pressure drop due to the dry packing and due to the liquid presence. It depends on liquid and gas flow rates, liquid and gas densities, liquid viscosity, gas velocity, dry packing factor (Fpd), as is shown from Eqs. (A.26a)–(A.26d).

$$\Delta P_z = 0.8169\left[\left(7.4\times10^{-8}\mathrm{Gf}_z^2 10^{2.710^{-5}\mathrm{Lf}_z}\right) + \left(0.4\,(\mathrm{Lf}_z/20000)^{0.1}\left(7.4\times10^{-8}\mathrm{Gf}_z^2(10)^{2.7\times10^{-5}\,\mathrm{Lf}_z}\right)^4\right)\right] \tag{A.26a}$$

where Gf_z (lb/h ft^2)and Lf_z (lb/h ft^2) are the gas and liquid loading packing factors and are computed as follows:

$$\mathrm{Gf}_z = 986\times\left(\frac{G'_z}{(\rho_z^G)^{0.5}3600}\right)\times\left(\frac{\mathrm{Fpd}}{20}\right)^{0.5}\times(10)^{0.3}\times\rho_z^G \quad P_{op}>1\,\text{atm} \tag{A.26b}$$

$$\mathrm{Lf}_z = L'_z\left(\frac{62.4}{\rho_z'^L}\right)\left(\frac{20}{\mathrm{Fpd}}\right)^{0.5}\left(\frac{\mu_z^L}{1000}\right)^{0.1} \quad P_{op}>1\text{ atm and Fpd} < 200 \tag{A.26c}$$

$$\mathrm{Lf}_z = L'_z\left(\frac{62.4}{\rho_z^L}\right)\left(\frac{\mathrm{Fpd}}{20}\right)^{0.5}\left(\frac{\mu_z^L}{1000}\right)^{0.2} \quad P_{op}>1\text{ atm and Fpd}>200 \tag{A.26d}$$

G' and L' are gas and liquid mass velocities (lb/h·ft^2), ρ'^G and ρ'^L are gas and liquid mass densities (lb/ft^3) and μ^L is the liquid viscosity (kg/m s).

Finally, the model includes correlations to compute fluid properties (vapor pressure, density, viscosity, enthalpies and diffusivity) which are taken from different specialized literature and are valid for a wide range of operating conditions.

Condenser [COND]

Mass and energy balances

$$G_z y_{i,z} - L_C x_{i,C} - G_C y_{j,C} = 0 \quad \forall i,j \quad z = Z \tag{A.27}$$

$$G_z\left(H_z^G + (\Delta H_R)_z + (\Delta H_{H_2O})_z\right) - L_C H_C^L - G_C\left(H_C^G + \Delta H_{H_2O,C}\right) - Q_C = 0 \quad z = Z \tag{A.28}$$

Phase equilibrium relationship

$$y_{j,C}\varphi_{j,C}P_C = p_i x_{i,C} \tag{A.29}$$

$$y_{jC} = y_{jC}^* \tag{A.30}$$

Reboiler [REB]

Mass and energy balances

$$L_z x_{i,z} - L_R x_{i,R} + G_R y_{j,R} = 0 \quad z = 1 \tag{A.31}$$

$$L_z H_z^L + Q_R - L_R H_R^L - G_R\left(H_R^G + (\Delta H_R)_R + (\Delta H_{H_2O})_R\right) = 0 \quad z = 1 \tag{A.32}$$

Phase equilibrium relationship

$$y_{CO_2,R} \quad \varphi_{CO_2,R}P_R = H_{CO_2,R}[CO_2]_R \tag{A.33}$$

$$y_{H_2O,R} \quad \varphi_{H_2O,R}P_R = p_{H_2O,R}x_{H_2O,R} \tag{A.34}$$

$$y_{j,R} = y_{j,R}^* \tag{A.35}$$

Reboiler and condenser units are modeled as equilibrium stages ($\eta = 1$), therefore similar equations to column stages are considered.

Heat exchangers (LAC and ECO)

Mass and energy balances

$$x_{i,RC}L_{RC} = x_{i,RH}L_{RH} \tag{A.36}$$

$$x_{i,R}L_R = x_{i,L}L_L = x_{i,LC}L_{LC} \tag{A.37}$$

$$Q_{la} = Q_{ECO} + Q_{LAC} = L_R H_R^L - L_{LC}H_{LC}^L \tag{A.38}$$

where Q_{la} (kJ/s) is the total cooling duty necessary to reach the desired inlet temperature to the top of absorber unit. A part of this energy (Q_{ECO}) is transferred by the hot amine coming from the bottom of the absorber and the rest (Q_{LAC}) is transferred by using cooling water. The intermediate temperature T_L is dependent of the both exchanger's sizes.

Inequality constraints

The following inequality constraint takes into account the trade-off existing between the reduction of the water flow rate exit with CO_2 towards the liquefaction unit and the temperature of the fluid returning to the column, which should be high enough for good regeneration efficiency [15].

$$y_{H_2O,C} \leq 0.10 \tag{A.39}$$

All optimizations considered an upper bound to the water content into the gas stream leaving the condenser of 10 %. As expected, it reached its upper bound in all cases. Finally, the model also includes the following inequality constraints:

$$0.10 \leq \eta_z \leq 0.35 \tag{A.40}$$

$$0.65 \leq f_z \leq 0.70 \tag{A.41}$$

$$T_R \geq T_{RH} + 10 \tag{A.42}$$

References

[1] Zhang R, Purusha Bonnin-Nartker E, Farthing G, Ji L, Klidas M, Nelson M, et al. RSAT™ process development for post-combustion CO_2 capture: scale-up from laboratory and pilot test data to commercial process design. Energy Procedia 2011;4:1660–7.

[2] Singh P, vanSwaaij WPM, (Wim)Brilman DWF. Kinetics study of carbon dioxide absorption in aqueous solutions of 1,6-hexamethyldiamine (HMDA) and 1,6-hexamethyldiamine, N, N0 di-methyl (HMDA, N, N0). Chemical Engineering Science 2011;66:4521–32.

[3] Mangalapally HP, Notz R, Hoch S, Asprion N, Sieder G, Garcia H, et al. Pilot plant experimental studies of post combustion CO_2 capture by reactive absorption with MEA and new solvents. Energy Procedia 2009;1(1):963–70.

[4] Kim I, Svendsen HF. Heat of absorption of carbon dioxide (CO_2) in mono-ethanolamine (MEA) and 2-(aminoethyl) ethanolamine (AEEA) solutions. Ind. Eng. Chem. Res. 2007;46:5803–9.

[5] Hasib-ur-Rahman M, Siaj M, Larachi F. Ionic liquids for CO_2 capture—development and progress. Chemical Engineering and Processing 2010;49:313–22.

[6] Rayer AV, Sumon KZ, Henni A, Tontiwachwuthikul P. Kinetics of the reaction of carbon dioxide (CO_2) with cyclic amines using the stopped-flow technique. Energy Procedia 2011;4:140–7.

[7] vanHolst J, Versteeg GF, Brilman DWF, Hogendoorn JA. Kinetic study of CO_2 with various amino acid salts in aqueous solution. Chemical Engineering Science 2009;64:59–68.

[8] Feng Qin F, Wang S, Hartono A, Svendsen HF, Chen C. Kinetics of CO_2 absorption in aqueous ammonia solution. International Journal of Greenhouse Gas Control 2010;4:729–38.

[9] Li H, Wilhelmsen Ø, Yuexia Lv, Wang W, Yan J. Viscosities, thermal conductivities and diffusion coefficients of CO_2 mixtures: review of experimental data and theoretical models. International Journal of Greenhouse Gas Control 2001;5(5):1119–39.

[10] Sakwattanapong R, Aroonwilas A, Veawab A. Reaction rate of CO_2 in aqueous MEA-AMP solution: experiment and modeling. Energy Procedia I 2009:217–24.

[11] Gong Y, Wang Z, Wang S. Experiments and simulation of CO_2 removal by mixed amines in a hollow fiber membrane module. Chemical Engineering and Processing: Process Intensification 2008;45(8):652–60.

[12] Dugas ER. Pilot Plant Study of Carbon Dioxide Capture by Aqueous onoethanolamine. M.S.E. Thesis, University of Texas at Austin; 2006.

[13] Plaza JM, Rochelle GT. Modeling pilot plant results for CO_2 capture by aqueous piperazine. Energy Procedia 2011;4:1593–600.

[14] Kale C, Tönnies I, Hasse H, Górak A. Simulation of reactive absorption: model validation for CO_2–MEA system. Computer Aided Chemical Engineering 2011; 29:61–5.

[15] Mofarahi M, Khojasteh Y, Khaledi H, Farahnak A. Design of CO_2 absorption plant for recovery of CO_2 from flue gases of gas turbine. Energy 2008;33(8): 1311–9.

[16] Bernier E, Maréchal F, Samson R. Multi-objective design optimization of a natural gas-combined cycle with carbon dioxide capture in a life cycle perspective. Energy 2010;35(2):1121–8.

[17] Möller BF, Genrup M, Assadi M. On the off-design of a natural gas-fired combined cycle with CO_2 capture. Energy 2007;32(4):353–9.

[18] Harkin T, Hoadley A, Hooper B. Using multi-objective optimisation in the design of CO2 capture systems for retrofit to coal power stations. Energy 2012;41(1):228–35.

[19] Geuzebroek FH, Schneiders LHJM, Kraaijveld GJC, Feron PHM. Exergy analysis of alkanolamine-based CO_2 removal unit with AspenPlus. Energy 2004; 29(9–10):1241–8.

[20] Pérez-Fortes M, Bojarski AD, Velo E, Nougués JM, Puigjaner L. Conceptual model and evaluation of generated power and emissions in an IGCC plant. Energy 2009;34(10):1721–32.

[21] Aroonwilas A, Chakma A, Tontiwachwuthikul P, Veawab A. Mathematical modelling of mass-transfer and hydrodynamics in CO_2 absorbers packed with structured packings. Chemical Engineering Science 2003;58(17):4037–53.

[22] Dorao CA, Tobiesen FA, Fernandino M. An improved flowsheet simulation approach for advanced CO_2 absorption process design and optimization. Energy Procedia 2009;1(1):4257–64.
[23] Sipöcz N, Tobiesen FA, Assadi M. The use of artificial neural network models for CO_2 capture plants. Applied Energy 2011;88(7):2368–76.
[24] Tobiesen FA, Juliussen O, Svendsen HF. Experimental validation of a rigorous desorber model for CO_2 post-combustion capture. Chemical Engineering Science 2008;63(10):2641–56.
[25] Khan FM, Krishnamoorthi V, Mahmud T. Modelling reactive absorption of CO_2 in packed columns for post-combustion carbon capture applications. Chemical Engineering Research and Design 2011;89(9):1600–8.
[26] Oexmann J, Hasenbein C, Kather A. Semi-empirical model for the direct simulation of power plant with integrated post-combustion CO_2 capture processes by wet chemical absorption. Energy Procedia 2011;4:1276–85.
[27] Cormos AM, Gaspar J, Agachi PS. Evaluation of CO_2 absorption–desorption cycle by dynamic modeling and simulation. Computer Aided Chemical Engineering 2011;29:1185–9.
[28] Zhou Q, Wu Y, Chan CW, Tontiwachwuthikul P. From neural network to neuro-fuzzy modeling: applications to the carbon dioxide capture process. Energy Procedia 2011;4:2066–73.
[29] Pellegrini G, Strube R, Manfrida G. Comparative study of chemical absorbents in postcombustion CO_2 capture. Energy 2010;35:851–7.
[30] Liang ZH, Sanpasertparnich T, Tontiwachwuthikul PPT, Gelowitz D, Idem R. Part 1: design, modeling and simulation of post-combustion CO_2 capture systems using reactive solvents. Carbon Management 2011;2(3):265–88.
[31] Rodríguez N, Mussati S, Scenna N. Optimization of post-combustion CO_2 process using DEA–MDEA mixtures. Chemical Engineering Research and Design 2011;89(9):1763–73.
[32] Mores P, Scenna N, Mussati S. Post-combustion CO_2 capture process: equilibrium stage mathematical model of the chemical absorption of CO_2 into monoethanolamine (MEA) aqueous solution. Chemical Engineering Research and Design 2011;89(9):1587–99.
[33] Lawal A, Wang M, Stephenson P, Yeung H. Dynamic modeling and simulation of CO_2 chemical absorption process for coal-fired power plants. Computer Aided Chemical Engineering 2009;27:1725–30.
[34] Brooke A, Kendrick D, Meeraus A. GAMS – a user's guide (release 2.25). San Francisco, CA: The Scientific Press; 1996.
[35] Drud AS. CONOPT, A GRG code for large scale nonlinear optimization. Reference manual. Bagsvaerd, Denmark: ARKI Consulting and Development A/S; 1992.
[36] Onda K, Takeuchi H, Okumoto Y. Mass transfer coefficients between gas and liquid phases in packed columns. Journal of Chemical Engineering of Japan 1968;1:56–62.
[37] Bravo JL, Fair JR. Generalized correlation for mass transfer in packed distillation columns. Industrial & Engineering Chemistry Process Design and Development 1982;21:162–70.
[38] Oyenekan B. Modeling of strippers for CO2 capture by aqueous amines. Ph.D. Dissertation, University of Texas at Austin; 2007.
[39] Hilliard M.D. A predictive thermodynamic model for an aqueous blend of potassium carbonate, piperazine and monoethanolamine for carbon dioxide capture from flue gas. Ph.D. Dissertation, University of Texas of Austin; 2008.
[40] Aboudheir A, Tontiwachwuthikul P, Chakma A, Idem R. Kinetic of reactive absorption of carbon dioxide in high CO_2-loaded, concentrated aqueous monoethenolamine solutions. Chemical Engineering Science 2003;58:5195–210.
[41] Liu Y, Zhang L, Watanasiri S. Representing vapor-liquid equilibrium for an aqueous MEA–CO_2 system using the electrolyte nonrandom-two-liquid model. Industrial & Engineering Chemistry Research 1999;38:2080–90.
[42] Peng DY, Robinson DB. A new two constant equation of state. Industrial Engineering Chemical Fundamentals 1976;15:59–64.
[43] Greer T. Modeling and simulation of post combustion CO2 capturing. Ph. D. Thesis, Telemark University College, Faculty of Technology, Porsgrunn, Norway; 2008.
[44] Leva M. Reconsider packed-tower pressure-drop correlations. Chemical Engineering Progress 1992;88:65–72.
[45] Kucka L, Kenig EY, Górak A. Kinetics of the gas–liquid reaction between carbon dioxide and hydroxide ions. Industrial & Engineering Chemistry Research 2002;41:5952–7.
[46] Robbins L. Improved pressure drop prediction with a new correlation. Chemical Engineering Progress 1991:87–91.